

# Is structure based drug design ready for selectivity optimization?

<sup>3</sup> Steven K. Albanese<sup>1,2</sup>, John D. Chodera<sup>2</sup>, Simon Peng<sup>3</sup>, Robert Abel<sup>3</sup>, Lingle Wang<sup>3\*</sup>

<sup>4</sup> <sup>1</sup>Louis V. Gerstner, Jr. Graduate School of Biomedical Sciences, Memorial Sloan Kettering Cancer  
<sup>5</sup> Center, New York, NY 10065; <sup>2</sup>Computational and Systems Biology Program, Sloan Kettering  
<sup>6</sup> Institute, Memorial Sloan Kettering Cancer Center, New York, NY 10065; <sup>3</sup>Schrödinger, New York,  
<sup>7</sup> NY 10036

<sup>8</sup> \*For correspondence: [lingle.wang@schrodinger.com](mailto:lingle.wang@schrodinger.com) (LW)

## Abstract

Alchemical free energy calculations are now widely used to drive or maintain potency in small molecule lead optimization, where the binding affinity to a protein target can be computed—in well-behaved cases—to roughly 1 kcal/mol inaccuracy, which is believed to primarily stem from force field errors. Despite this, the potential to use free energy calculations to drive optimization of compound *selectivity* among two similar targets has been relatively unexplored. In the most optimistic scenario, the similarity of binding sites might lead to a fortuitous cancellation of force field errors and allow selectivity to be predicted more accurately than affinity. Here, we assess the accuracy with which selectivity can be predicted in the context of small molecule kinase inhibitors, considering the very similar binding sites of human kinases CDK2 and CDK9, as well as another series of ligands attempting to achieve selectivity between the more distantly related kinases CDK2 and ERK2. Using a novel Bayesian analysis approach, we separate force field error from statistical error and quantify the correlation in force field errors between selectivity targets. We find that, in the closely related CDK2/CDK9 case, a high correlation in force field errors suggests free energy calculations can have significant impact in aiding chemists in achieving selectivity, while in more distantly related kinases (CDK2/ERK2), limited correlation in force field errors reduces the ability for free energy calculations to aid selectivity optimization. In both cases, the correlation in force field error suggests that longer simulations are beneficial to properly balance statistical error with systematic error to take full advantage of the increase in accuracy in selectivity prediction possible due to fortuitous cancellation of error.

Free energy methods have proven useful in aiding structure-based drug design by driving the optimization or maintenance of potency in lead optimization. Alchemical free energy calculations allow for prediction of ligand binding free energies, including all enthalpic and entropic contributions [1]. Advances in atomistic molecular mechanics forcefields and free energy methodologies [2–5] have allowed free energy methods to reach a level of accuracy sufficient for predicting ligand potencies [6]. Free energy methods have been applied prospectively to develop inhibitors for Tyk2 [7], Syk [8], BACE1 [9], GPCRs [10], and HIV protease [11]. A recent large-scale review found that the use of FEP+ [12] to predict potency for 92 different projects and 3021 compounds found a median RMSE of 1 kcal/mol [13].

Selectivity is an important consideration in drug design

In addition to maintaining or optimizing potency, free energy methods can be applied to predicting the selectivity of a ligand between two or more targets. Selectivity is an important property to consider in drug development, either in the pursuit of a maximally selective inhibitor [14, 15] or in pursuit a polypharmacological agent [16–20], to avoid on-target toxicity (arising from inhibition of the intended target) [21] and off-target toxicity (arising from inhibition of unintended targets) [22, 23]. In either paradigm, considering the

43 selectivity of a compound is complicated by the biology of the target. For example, kinases exist as nodes  
 44 in complex signaling networks [24, 25] with feedback inhibition and cross-talk between pathways. Careful  
 45 consideration of which off-targets are being inhibited can avoid off-target toxicity due to alleviating feedback  
 46 inhibition and inadvertently reactivating the targeted pathway [24, 25], or the upregulation of a secondary  
 47 pathway by alleviation of cross-talk inhibition [26, 27]. Off-target toxicity can also be caused by inhibiting  
 48 unrelated targets, such as gefitinib, an EGFR inhibitor, inhibiting CYP2D6 [22] and causing hepatotoxicity  
 49 in lung cancer patients. In a cancer setting, on-target toxicity can be avoided by considering the selectivity  
 50 for the oncogenic mutant form of the kinase over the wild type form of the kinase [28–30], demonstrated  
 51 by number of first generation EGFR inhibitors. Selectivity considerations can also lead to beneficial effects:  
 52 Imatinib, initially developed to target BCR-Abl fusion proteins, is also approved for treating gastrointestinal  
 53 stromal tumors (GIST) [31] due to its activity against receptor tyrosine kinase KIT.

54 Use of physical modeling to predict selectivity is relatively unexplored

55 While predicting selectivity is important for drug discovery, but the utility of free energy methods for  
 56 predicting this property is relatively unexplored. If there is fortuitous cancellation of errors for closely  
 57 related systems, free energy methods may be much more accurate than expected given the errors made in  
 58 predicting the potency for each individual target. The selectivity of Imatinib for Abl kinase over Src [32, 33]  
 59 and within a family of non-receptor tyrosine kinases [34] has been studied extensively using molecular  
 60 dynamics and free energy calculations. This work focuses on understanding the role reorganization energy  
 61 plays in the exquisite selectivity of imatinib for Abl over Src despite high similarity between cocrystallized  
 62 binding mode and kinase conformations, and does not touch on the evaluation of the accuracy of these  
 63 methods, or their application to drug discovery on congeneric series of ligands. Previous work predicting the  
 64 selectivity of three bromodomain inhibitors across the bromodomain family achieved promising accuracy  
 65 for single target potencies of roughly 1 kcal/mol, but does not explicitly evaluate any selectivity metrics [35]  
 66 or look at correlation in the errors made for each bromodomain.

67 Kinases are an interesting and particularly challenging model system for selectivity predictions  
 68 Kinases are a useful model system to work with for assessing the utility of free energy calculations to predict  
 69 selectivity. With the approval of imatinib for the treatment of chronic myelogenous leukemia in 2001,  
 70 targeted small molecule kinase inhibitors (SMKIs) have become a major class of therapeutics in treating  
 71 cancer and other diseases. Currently, there are 43 FDA-approved SMKIs [36], and it is estimated that  
 72 kinase targeted therapies account for as much as 50% of current drug development [37], with many more  
 73 compounds currently in clinical trials. While there have been a number of successes, the current stable of  
 74 FDA-approved kinase inhibitors targets only a small number of kinases implicated in disease, and the design  
 75 of new selective kinase inhibitors remains a significant challenge. Achieving desired selectivity profiles is  
 76 particularly difficult for kinase targets, making them a system where physical modelling has the potential for  
 77 a large impact. Achieving selective inhibition of kinases is challenging as there are more than 518 protein  
 78 kinases [38, 39] with a highly conserved ATP binding site that is targeted by the majority of SMKIs [40]. While  
 79 kinase inhibitors have been designed to target kinase-specific subpockets and binding modes to achieve  
 80 selectivity [41–46], previous work has shown that both Type I (binding to the active, DFG-in conformation) and  
 81 Type II (binding to the inactive, DFG-out conformation) inhibitors display a wide variety of selectivities [47, 48],  
 82 often exhibiting significant binding to a number of other targets in addition to their primary target. Even  
 83 FDA-approved inhibitors—often the result of extensive drug development programs—bind to a large number  
 84 of off-target kinases [49]. Kinases are also targets of interest for developing polypharmacological compounds,  
 85 or inhibitors that are specifically designed to inhibit multiple kinase targets. Resistance to MEK inhibitors  
 86 in KRAS-mutant lung and colon cancer has been shown to be driven by HER3 upregulation [50], providing  
 87 rational for dual MEK/ERBB family inhibitors. Similarly, combined MEK and VEGFR1 inhibition has been  
 88 proposed as a combinatorial approach to treat KRAS-mutant lung cancer [51]. Developing inhibitors with  
 89 the desired polypharmacology means navigating more complex selectivity profiles. In well-behaved kinase  
 90 systems, free energy calculations potency predictions have achieved mean unsigned errors of less than 1.0  
 91 kcal/mol [7, 12], suggesting that kinases can be computationally tractable as well as clinically interesting.

92 Assessing the ability of alchemical free energy methods to predict selectivity  
 93 We anticipate difficulty in predicting selectivity if the errors in the alchemical free energy calculations for two  
 94 targets are largely uncorrelated, or even anticorrelated. However, correlation in the forcefield errors of the  
 95 free energies for the two targets could lead to a fortuitous cancellation of errors in predicting the selectivity  
 96 between targets, making selectivity predictions *more* accurate than potency predictions. Such correlation  
 97 could occur because the same chemical elements appear in the ligand and in highly related binding sites.  
 98 Here, we investigate the magnitude of this correlation ( $\rho$ ) and the utility of alchemical free energy calculations  
 99 for the prediction of selectivity, hereafter taken to mean the  $\Delta\Delta G$  in binding free energies of the same  
 100 compound for two targets. We employed state of the art relative free energy calculations [12, 13] to predict  
 101 the selectivities of two different congeneric ligand series [52, 53], as well as present a simple numerical  
 102 model to quantify the potential speed up in selectivity optimization expected for different combinations  
 103 of per target errors and correlation coefficient values. To tease out the effects of a limited number of  
 104 experimental measurements, we develop a new Bayesian approach to quantify the uncertainty in the  
 105 correlation coefficient in the predicted change in selectivity on ligand modification, incorporating all sources  
 106 of uncertainty and correlation in the computation to separate statistical from force field error. We find  
 107 that in the closely related systems of CDK2 and CDK9, a high correlation of force field errors suggests that  
 108 free energy methods can have a significant impact on speeding up selectivity optimization. In the more  
 109 distantly related case (CDK2/ERK2), limited correlation hampers the ability for free energy methods to speed  
 110 up selectivity optimization.

## 111 Methods

### 112 Numerical model of selectivity

113 To model the impact correlation would have on the expected uncertainty for selectivity predictions,  $\sigma_{selectivity}$   
 114 was calculated using Equation 1 for 1000 evenly spaced values of the correlation coefficient ( $\rho$ ) from 0 to 1,  
 115 for a number of combinations of per target errors ( $\sigma_{target1}$  and  $\sigma_{target2}$ )

$$\sigma_{selectivity} = \sqrt{\sigma_{target1}^2 + \sigma_{target2}^2 - 2\rho\sigma_{target1}\sigma_{target2}} \quad (1)$$

116 The speed up in selectivity optimization that could be expected from using free energy calculations  
 117 of a particular per target error ( $\sigma_{selectivity}$ ) was quantified as follows using NumPy (v 1.14.2). An original, true  
 118 distribution for the change in selectivity of 200000000 new compounds proposed with respect to a  
 119 reference compound was modeled as a normal distribution centered around 0 with a standard deviation of 1  
 120 kcal/mol. This assumption was made on the basis that the majority of selectivity is driven by the scaffold, and  
 121 R group modifications will do little to drive changes in selectivity. The 1 kcal/mol distribution is supported by  
 122 the standard deviations of the selectivity in the experimental datasets referenced in this work, which are all  
 123 less than, but close, to 1 kcal/mol.

124 Each of these proposed compounds were "screened" by a free energy calculation technique with a per  
 125 target error ( $\sigma_{target}$ ) of 1 kcal/mol [12] and a specified correlation coefficient  $\rho$ . A  $\sigma_{selectivity}$  was calculated  
 126 according to Equation 1. The noise of the computational method was modeled as a normal distribution  
 127 centered around 0 with a standard deviation of  $\sigma_{selectivity}$  and added to the "true" change in selectivity. Any  
 128 compound predicted to have an improvement in selectivity of 1.4 kcal/mol (1 log unit) would then be made  
 129 and have its selectivity experimentally measured. The speedup value for each value of  $\rho$  is calculated as the  
 130 proportion of compounds made with a true selectivity gain of 1.4 kcal/mol divided by the proportion of  
 131 compounds with a 1.4 kcal/mol improvement in the original distribution, where all of the compounds were  
 132 made.

133 Finally, this process was repeated for a 100x (2.8 kcal/mol, 2 log unit) selectivity optimization and 50  
 134 linearly spaced values of the correlation coefficient ( $\rho$ ) between 0 and 1, for four values of  $\sigma_{selectivity}$ , and  
 135 40000000 compounds in the original distribution.

### 136 Structure Preparation

137 Structures from the Shao [52] and Hole [54], and Blake [53] papers were downloaded from the PDB [55], selecting  
 138 structures with the same co-ligand crystallized. For the Shao dataset, 4BCK (CDK2) and 4BCI (CDK9) were

selected, which have ligand 12c cocrystallized. For the Blake dataset, 5K4J (CDK2) and 5K4I (ERK2) were selected, cocrystallized with ligand 21. The structures were prepared using Schrodinger's Protein Preparation Wizard [56] (release 2017-3). This pipeline modeled in internal loops and missing atoms, added hydrogens at the reported experimental pH (7.0 for the Shao dataset, 7.3 for the Blake dataset) for both the protein and the ligand. All crystal waters were retained. The ligand was assigned protonation and tautomer states using Epik at the experimental pH $\pm$ 2, and hydrogen bonding was optimized using PROPKA at the experimental pH $\pm$ 2. Finally, the entire structure was minimized using OPLS3 with an RMSD cutoff of 0.3Å.

#### 146 Ligand Pose Generation

Ligands were extracted from the publication entries in the BindingDB as 2D SMILES strings. 3D conformations were generated using LigPrep with OPLS3 [57]. Ionization state was assigned using Epik at experimental pH $\pm$ 2. Stereoisomers were computed by retaining any specified chiralities and varying the rest. The tautomer and ionization state with the lowest epik state penalty was selected for use in the calculation. Ligand poses were generated by first aligning to the co-crystal ligand using the Largest Common Bemis-Murcko scaffold with fuzzy matching (Schrodinger 2017-4). Ligands that were poorly aligned or failed to align were then aligned using Maximum Common Substructure (MCSS). Finally, large R-groups were allowed to sample different conformations using MM-GBSA with a common core restrained. VSGB solvation model was used with the OPLS3 forcefield. No flexible residues were defined for the ligand.

#### 156 Free Energy Calculations

The FEP+ panel (Maestro release 2017-4) was used to generate perturbation maps. FEP+ calculations were run using the FEP+ panel from Maestro release 2018-3, using the parameters from the version of OPLS3e that shipped with the 2018-3 release. Any missing ligand torsions were fit using the automated FFbuilder protocol [58]. Custom charges were assigned using the OPLS3e forcefield using input geometries, according to the automated FEP+ workflow released in 2018-3. Neutral perturbations were run for 15ns per replica, using an NPT ensemble and water buffer size of 5Å. The SPC water model was used. A GCMC solvation protocol was used to sample buried water molecules in the binding pocket prior to the calculation, which discards any retained crystal waters.

#### 165 Charge Change Free Energy Calculations

For ligands where a protonation state change was expected to be relevant to binding based on a small state penalty, Jaguar pKa prediction calculations [59] were run to identify protonation state changes with pKas within 1 log unit of the experimental pH. The predicted pKas for one ligand (Shao 12b, 7.84) was within this range. To account for this, a pKa correction was performed. For this ligand, a separate perturbation map containing ligands 12a, 12c, 12b (neutral) and 12b (charged) was run for 30ns per replica using a post-calculation Coulombic charge correction. Each charge change perturbation edge was run with a 150mM NaCl concentration. The pKa correction was performed using Equation 2:

$$\Delta\Delta G_{corrected} = \Delta\Delta G_{uncorrected} - RT \log \left( \frac{10^{pK_a-pH} + 1}{e^{\frac{\Delta G_{neutral}-\Delta G_{charged}}{RT}} * (10^{pK_a-pH} + 1)} \right) \quad (2)$$

173 ΔΔG for each edge in perturbation map with 12a, 12c and 12b (neutral) was updated using the correction  
174 above and merged into the final map.

#### 175 Statistical Analysis of FEP+ calculations

176 Each FEP+ calculation has a reported mean unsigned error (MUE) and root mean squared error (RMSE) with  
177 a bootstrapped 95% confidence interval. The MUE was calculated according Equation 3, while the RMSE was  
178 calculated according to Equation 4.

$$MUE = \frac{\sum_0^n |\Delta G_{calc} - \Delta G_{exp}|}{n} \quad (3)$$

$$RMSE = \frac{\sqrt{\sum_0^n (\Delta G_{calc}^2 - \Delta G_{exp}^2)}}{n} \quad (4)$$

179     Each RMSE and MUE is reported with a 95% confidence interval calculated from 10000 replicates of a  
 180 choose-one-replace bootstrap protocol on the  $\Delta G$  values reported to account for the finite sample size of the  
 181 ligands. The code used to bootstrap these values is available on github: <https://github.com/choderlab/selectivity>

182     Quantification of the correlation coefficient  $\rho$

183     To quantify  $\rho$ , we built a Bayesian graphical model using pymc3 (v. 3.5) [60] and theano (v 1.0.3) [61], which  
 184 has been made available on Github. For each phase (complex and solvent), the absolute free energy ( $G$ )  
 185 of ligand  $i$  was treated as a normal distribution (Equation 5). For each set of calculations, one ligand was  
 186 chosen as the reference, and pinned to 0, with a standard deviation of 1 kcal/mol in order to improve the  
 187 efficiency of sampling from the model.

$$G_{i,target}^{phase} = \mathcal{N}(\mu = 0, sd = 25.0 \text{ kcal/mol}) \quad (5)$$

188     For each edge of the FEP map (ligand  $i \rightarrow$  ligand  $j$ ), there is a contribution from dummy atoms, that was  
 189 modeled as in Equation 6.

$$c_{i,j} = \mathcal{N}(\mu = 0, sd = 25.0 \text{ kcal/mol}) \quad (6)$$

190     The model was restrained by including data from the FEP+ calculation.

$$\Delta G_{phase, ij, target}^{BAR} = \mathcal{N}(G_{j,target}^{phase} - G_{i,target}^{phase}, \delta^2 \Delta G_{phase, ij, target}^{BAR}, observed = \Delta G_{phase, ij, target}^{calc}) \quad (7)$$

191     Where  $\delta^2 \Delta G_{phase, ij, target}^{BAR}$  is the reported BAR uncertainty from the calculation, and  $\Delta G_{phase, ij, target}^{calc}$  is the  
 192 BAR estimate of the free energy for the perturbation between ligands  $i$  and  $j$  in a given phase.

193     From this, we can calculate the  $\Delta \Delta G_{target, ij}^{FEP}$  for each edge as in Equation 8:

$$\Delta \Delta G_{target, ij}^{FEP} = \Delta G_{complex, ij, target}^{BAR} - \Delta G_{solvent, ij, target}^{BAR} \quad (8)$$

194     To model the way an offset is calculated for the  $\Delta G$  reported by the FEP+ panel in Maestro:

$$\text{offset} = \frac{\sum^n G_{i,target}^{complex} - G_{i,target}^{solvent}}{n} - \frac{\sum^n \Delta G_i^{exp}}{n} \quad (9)$$

195     The offset was added to each  $\Delta G_i^{BAR}$  to calculate  $\Delta G_i^{sch}$ .

196     The experimental binding affinity was treated as a true value ( $\Delta G_{i,target}^{true}$ ) corrupted by experimental  
 197 uncertainty, which is assumed to be 0.3 kcal/mol [6], with the values reported in the papers ( $\Delta G_{i,target}^{obs}$ ) treated  
 198 as observations from this distribution (Equation 10)

$$\Delta G_{i,target}^{exp} = \mathcal{N}(\Delta G_{i,target}^{true}, 0.3 \text{ kcal/mol}, observed = \Delta G_{i,target}^{obs}) \quad (10)$$

199      $\Delta G_{i,target}^{true}$  was assigned a weak normal prior, as in equation 11.

$$\Delta G_{i,target}^{true} = \mathcal{N}(0, 50 \text{ kcal/mol}) \quad (11)$$

200     The error for a given ligand was calculated as in Equation 12.

$$\epsilon_i = \Delta G_i^{sch} - \Delta G_i^{true} \quad (12)$$

201     From these  $\epsilon$  values, we calculated the correlation coefficient,  $\rho$  as in Equation 13.

$$\rho = \frac{cov(\epsilon_{target1}, \epsilon_{target2})}{\sigma_{target1} \sigma_{target2}} \quad (13)$$

202     Where  $\sigma$  is the standard deviation of  $\epsilon$ . To quantify  $\rho$  for the CDK2/ERK2 calculations, the default NUTS  
 203 sampler with jitter+adapt\_diag initialization, 1000 tuning steps, and a target accept probability of 0.8 was  
 204 used to draw 10000 samples from the model. The CDK2/CDK9 model was sampled 20000 times using default  
 205 NUTS sampler with jitter+adapt\_diag initialization and 3000 tuning steps.

206 **Results**

207 Free energy methods can be used to predict the selectivity of a compound  
 208 While ligand potency for a single target is often quantified as a free energy of binding ( $\Delta G_{\text{binding}}$ ), there are  
 209 a number of different metrics for quantifying the selectivity of a compound [62, 63]. Here, we propose  
 210 a more granular view of selectivity: the change in free energy of binding for a given ligand between two  
 211 different targets ( $\Delta\Delta G_{\text{selectivity}}$ ), which can be calculated as in Equation 14.  $\Delta\Delta G_{\text{selectivity}}$  is a useful measure of  
 212 compound selectivity once a single, or small panel, of off-targets have been identified.

$$\Delta\Delta G_{\text{selectivity}} = \Delta G_{\text{binding, target 2}} - \Delta G_{\text{binding, target 1}} \quad (14)$$

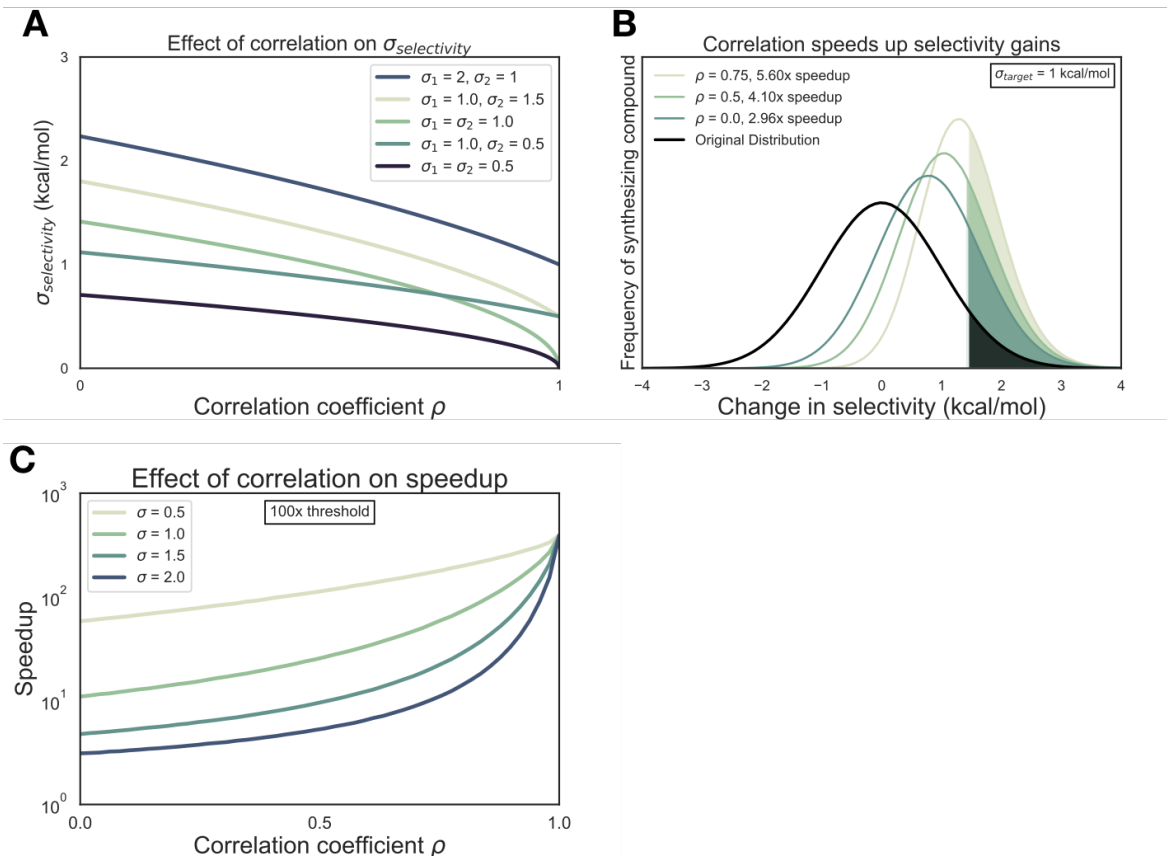
213 To predict the  $\Delta\Delta G_{\text{selectivity}}$  of a compound, we developed a protocol that uses a relative free energy  
 214 calculation (FEP+) [12] to run a map of perturbations between ligands in a congeneric series, as described  
 215 in depth in the methods section. The calculation is repeated for each target of interest, with identical  
 216 perturbations (edges) between each ligand (nodes). Each edge represents a relative free energy calculation  
 217 that quantifies the  $\Delta\Delta G$  between the ligands, or nodes. By using provided experimental data, we can convert  
 218 the  $\Delta\Delta G$  from each edge to a single potency value for each value against that target ( $\Delta G_{\text{target}}$ ). From this  
 219 sets of calculations, we can calculate a  $\Delta\Delta G_{\text{selectivity}}$  for each ligand given two targets of interest. Previous  
 220 work shows that FEP+ can achieve an accuracy ( $\sigma_{\text{target}}$ ) of roughly 1 kcal/mol when predicting potency, which  
 221 is a combination of systematic forcefield and random statistical error [12]. However, it is possible that  
 222 the forcefield component of that error may fortuitously cancel when computing  $\Delta\Delta G_{\text{selectivity}}$ , leading to a  
 223 selectivity uncertainty ( $\sigma_{\text{selectivity}}$ ) that is lower than would be expected.

224 Correlation of errors can make selectivity predictions more accurate and speed up ligand optimi-  
 225 zation

226 To demonstrate the potential impact correlation has on the uncertainty of selectivity predictions ( $\sigma_{\text{selectivity}}$ )  
 227 using alchemical free energy techniques, we created a simple numerical model following equation 1, which  
 228 takes into account each of the per target errors expected from the methodology as well as the correlation  
 229 in those errors. As seen in Figure 1A, if the per target errors ( $\sigma_1$  and  $\sigma_2$ ) are the same,  $\sigma_{\text{selectivity}}$  approaches  
 230 0 as the correlation coefficient ( $\rho$ ) approaches 1. If the error for the free energy method is not the same,  
 231  $\sigma_{\text{selectivity}}$  gets smaller but approaches a non-zero value as  $\rho$  approaches 1. To quantify the expected speedup  
 232 in selectivity optimization, we modeled the change in selectivity with respect to a reference compound for a  
 233 number of compounds a medicinal chemist might suggest as a normal distribution centered around 0 with a  
 234 standard deviation of 1 kcal/mol (Figure 1B, black curve), reflecting that most proposed changes would not  
 235 drive large changes in selectivity. Then, suppose that each compound is screened computationally with a  
 236 method free energy methodology with a per target ( $\sigma_{\text{target}}$ ) error of 1 kcal/mol, and all compounds predicted  
 237 to have a 1.4 kcal/mol improvement in selectivity are synthesized and experimentally tested (Figure 1B,  
 238 colored curves). The fold-change in the proportion of compounds that are made that have a true 1.4 kcal/mol  
 239 improvement in selectivity compared to the original distribution can be calculated as a surrogate for the  
 240 expected speedup. For a 1.4 kcal/mol selectivity improvement threshold (1 log unit), a correlation of 0.5  
 241 gives an expected speed up of 4.1x, which can be interpreted as 4.1x fewer compounds needing to be  
 242 made before achieving a 1 log unit improvement in selectivity. This process can be extended for the even  
 243 more difficult proposition of achieving a 2 log unit improvement in selectivity (Figure 1C), where 200-300x  
 244 speedups can be expected, depending on  $\sigma_{\text{target}}$  for the free energy methodology.

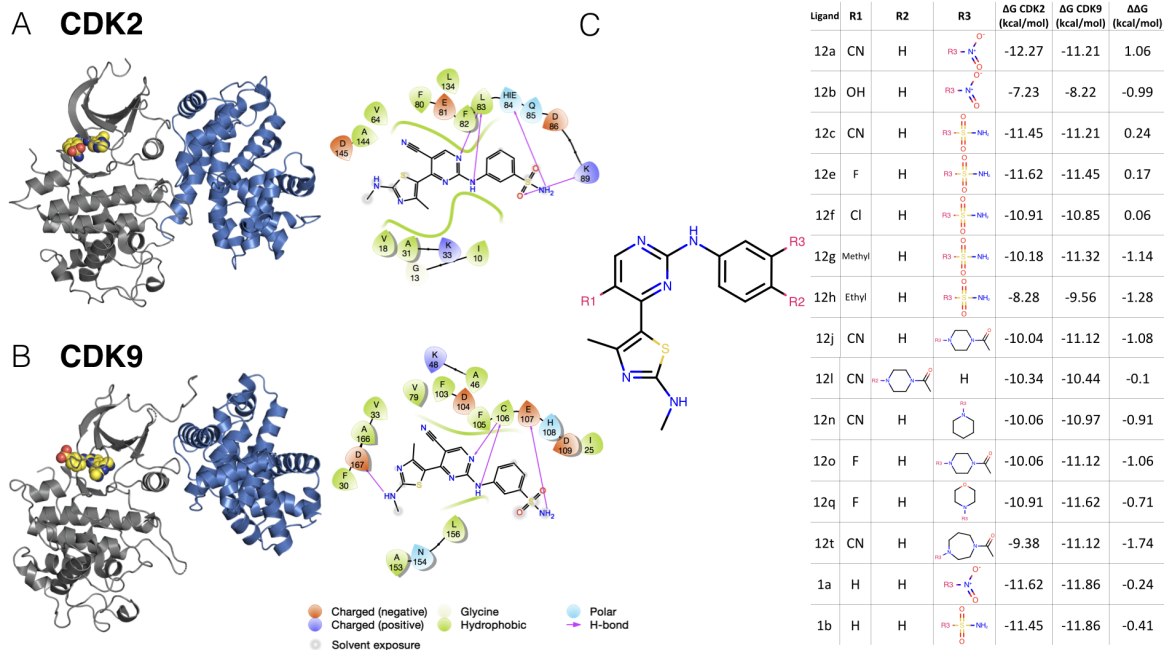
245 The CDK2 and CDK9 experimental dataset demonstrates the difficulty in achieving selectivity for  
 246 closely related kinases

247 To begin quantifying the correlation of errors in free energy predictions for selectivity, we set out to gather  
 248 datasets that met a number of criteria. We looked for datasets that contained binding affinity data for a  
 249 number of kinase targets and ligands, as well as having crystal structures for each target with the same  
 250 co-crystallized ligand. For the CDK2/CDK9 dataset [52], ligand 12c was cocrystallized with CDK2/cyclin A  
 251 (Figure 2A, left) and CDK9/cyclin T (Figure 2B, left), work that was published in a companion paper [54]. In  
 252 both CDK2 and CDK9, ligand 12c forms relatively few hydrogen bond interactions with the kinase. Each



**Figure 1. Free energy calculations speed up selectivity optimization**

(A) The effect of correlation on expected errors for predicting selectivity ( $\sigma_{selectivity}$ ) in kcal/mol. Each curve represents a different combination of target errors ( $\sigma_1$  and  $\sigma_2$ ). (B) The change in selectivity for molecules proposed by medicinal chemists optimizing a lead candidate can be modeled by a normal distribution centered on 0 with a standard deviation of 1 kcal/mol (black curve). Each green curve corresponds to the distribution of compounds made after screening for a 1 log unit (1.4 kcal/mol) improvement in selectivity with a free energy methodology with a 1 kcal/mol per target error and a particular correlation. The shade region of each curve corresponds to the compounds with a real 1 log unit improvement in selectivity. The speed up is calculated as the ratio of the percentage of compounds made with a real 1 log unit improvement to the percentage of compounds that would be expected in the original distribution. (C) The speedup (y-axis, log scale) expected for 100x (2 log units, 2.8 kcal/mol) selectivity optimization as a function of correlation coefficient  $\rho$ . Each curve corresponds to a different  $\sigma_{target}$  value.

**Figure 2. A CDK2/CDK9 selectivity dataset from Shao et al., 2013**

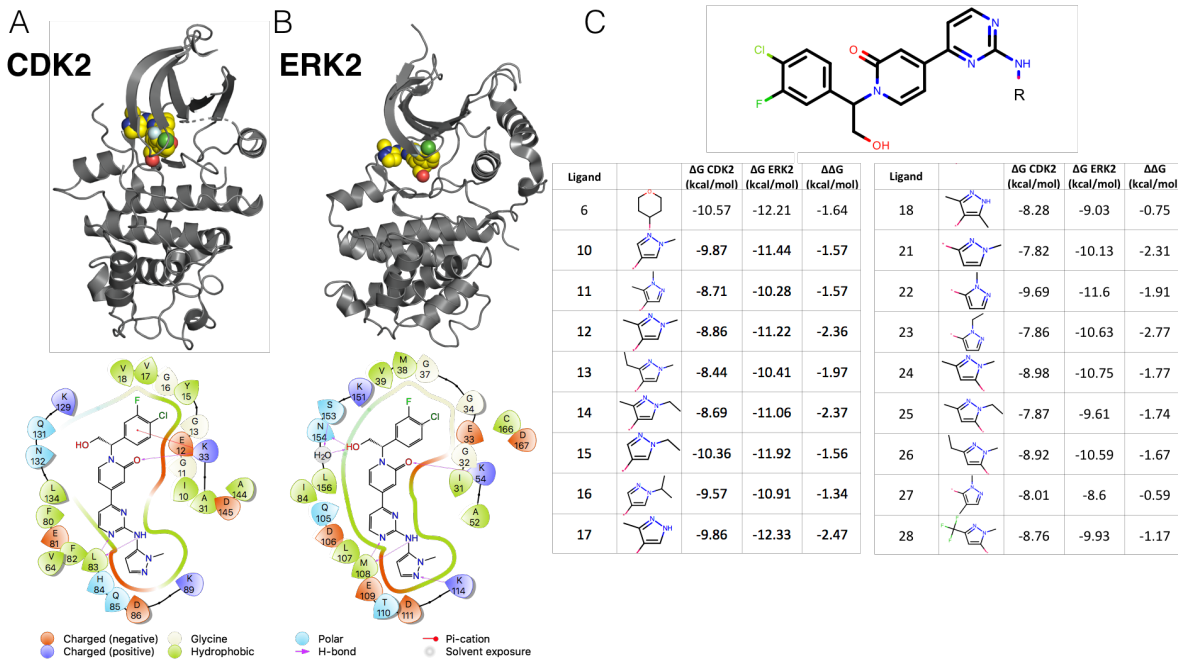
**(A)** (left) Crystal Structure (4BCK)[54] of CDK2 (gray ribbon) bound to ligand 12c (yellow spheres). Cyclin A is shown in blue ribbon (right) 2D ligand interaction map of ligand 12c in the CDK2 binding site. **(B)** (left) Crystal structure of CDK9 (4BCI)[54] (gray ribbon) bound to ligand 12c (yellow spheres). Cyclin T is shown in blue ribbon. (right) 2D ligand interaction map of ligand 12c in the CDK9 binding site. **(C)** (left) 2D structure of the common scaffold for all ligands in congeneric ligand series 12 from the publication (right) A table summarizing all R group substitutions as well as the published experimental binding affinities and selectivities[52].

kinase forms a set of hydrogen bonds between the ligand scaffold and a hinge residue (C106 in CDK9 and L83 in CDK2) that is conserved across all of the ligands in this series. CDK9, which has slightly lower affinity for ligand 12c (Figure 2C, right), forms a lone interaction between the sulfonamide of ligand 12c and residue E107. On the other hand, CDK2 forms interactions between the sulfonamide of ligand 12c and residues K89 and H84. The congeneric series of ligands contains a number of challenging perturbations, particularly at substituent point R3 (Figure 2C, left). Ligand 12i also presented a challenging perturbation, moving the 1-(piperazine-1-yl)ethanone from the *meta* to *para* location.

This congeneric series of ligands also highlights two of the challenges of working from publicly available data. First, the dynamic range of selectivity is incredibly narrow, with a mean  $\Delta\Delta G_{selectivity}$  (CDK9 - CDK2) of only -0.65 kcal/mol, and a standard deviation of 0.88 kcal/mol. Additionally, experimental uncertainties are not reported for the experimental measurements. Thus, for this and subsequent sets of ligands, the experimental uncertainty is assumed to be 0.3 kcal/mol based on previous work done to summarize uncertainty in experimental data [6, 64].

The CDK2 and ERK2 dataset achieves higher levels of selectivity for more distantly related kinases. The CDK2/ERK2 dataset from Blake *et al.*, 2016 also met the criteria described above. Crystal structures for both CDK2 (Figure 3A, top) and ERK2 (Figure 3B, top) were available with ligand 22 co-crystallized. Of note, CDK2 was not crystallized with cyclin A, despite cyclin A being included in the affinity assay reported in the paper [53]. CDK2 adopts a DFG-in conformation with the  $\alpha$ C helix rotated out, away from the ATP binding site and breaking the conserved salt bridge between K33 and E51 (Supp. Figure 1A), indicative of an inactive kinase [43, 65]. By comparison, the CDK2 structure from the CDK2/CDK9 dataset adopts a DFG-in conformation with the  $\alpha$ C helix rotated in, forming the ionic bond between K33 and E51 indicative of an active kinase, due to allosteric activation by cyclin A. While missing cyclins have caused problems for free

I probably need to either remove the reference to how closely related the kinases are, or come up with a way to quantify that - SKA

**Figure 3. CDK2 and ERK2 selectivity dataset from Blake et al., 2016**

**(A)** (top) Crystal structure of CDK2 (5K4j) shown in gray cartoon and ligand 22 shown in yellow spheres. (bot) 2D interaction map of ligand 22 in the binding pocket of CDK2 **(B)** (top) Crystal structure of ERK2 (5K4l) shown in gray cartoon with ligand 22 shown in yellow spheres. (bot) 2D interaction map of ligand 22 in the binding pocket of ERK2. **(C)** (top) Common scaffold for all of the ligands in the Blake dataset, with R denoting attachment side for substitutions. (bot) Table showing R group substitutions and experimentally measured binding affinities and selectivities. Ligand numbers correspond to those used in publication.

is there a good citation for this? 275  
energy calculations in prior work, it is possible that the fully active conformation contributes equally to 276 binding affinity for all of the ligands in the series, and the high accuracy of the potency predictions (Figure 4, 277 top left) is the result of fortuitous cancellation of errors. The binding mode for this series is similar between 278 both kinases. There is a set of conserved hydrogens bonds between the scaffold of the ligand and the 279 backbone of one of the hinge residues (L83 for CDK2 and M108 for ERK2). The conserved lysine (K33 for 280 CDK2 and K54 for ERK2), normally involved in the formation of a ionic bond with the  $\alpha$ C helix, forms a 281 hydrogen bond with the scaffold (Figure 4A and 4B, bottom) in both CDK2 and ERK2. However, in the ERK2 282 structure, the hydroxyl engages a crystallographic water as well as N154 in a hydrogen bond network that is 283 not present in the CDK2 structure. The congenic ligand series features a single substituent point, with the R 284 groups exposed to the solvent. This helps explain the extremely narrow distribution of selectivities, with a 285 mean selectivity of -1.74 kcal/mol (ERK2 - CDK2) and standard deviation of 0.56 kcal/mol. This suggests that 286 the selectivity is largely driven by the scaffold and unaffected by the R group substitutions.

287 FEP+ calculations show accurate potency predictions for ERK2/CDK2 and larger errors for CDK2/CDK9  
288 The FEP+ predictions of single target potencies ( $\Delta G$ ) showed good accuracy for the CDK2 and ERK2 dataset  
289 (Figure 4, top), with an RMSE of  $0.37^{0.57}_{0.16}$  and  $0.53^{0.81}_{0.22}$  kcal/mol, respectively. All of the CDK2 and ERK2 potencies  
290 were predicted within 1 log unit of the experimental value. The selectivity ( $\Delta \Delta G_{selectivity}$ ) predictions show  
291 an RMSE of  $0.81^{1.26}_{0.37}$  kcal/mol, with all of the predictions falling within 1 log unit of the experimental values  
292 (Figure 4, top right panel).. Despite the high accuracy of the predictions, the narrow dynamic range and high  
293 uncertainty from experiment and calculation obscures any signal in the data. The CDK2 and CDK9 datasets  
294 show higher errors in the potency predictions, with an RMSE of  $1.39^{2.05}_{0.58}$  and  $1.71^{2.61}_{0.61}$  kcal/mol respectively.  
295 There are a number of outliers that fall outside of 1 log unit from the experimental value. While the higher  
296 per target errors make predicting potency more difficult, the selectivity predictions show a much lower RMSE

297 of  $0.74_{0.31}^{1.25}$  kcal/mol. This suggests that some correlation in the error is leading to fortuitous cancellation of  
 298 systematic error, leading to more accurate than expected predictions of  $\Delta\Delta G_{selectivity}$ .

299 Correlation of forcefield errors accelerates selectivity optimization

300 To quantify the correlation coefficient ( $\rho$ ) of the forcefield errors in our calculations, we built a Bayesian  
 301 graphical model to separate the forcefield error from the statistical error, as described in the methods  
 302 section. Briefly, we modeled the absolute free energy ( $G$ ) of each ligand in each phase (complex and solvent)  
 303 as in equation 5. The model was chained to the FEP+ calculations by providing the  $\Delta G_{phase,ij,target}^{calc}$  as observed  
 304 data, as in equation 7. As in equation 8, the experimental data was modeled as a normal distribution centered  
 305 around the true free energy of binding ( $\Delta G_{i,target}^{true}$ ) corrupted by experimental error, which is assumed to  
 306 be 0.3 kcal/mol from previous work done to quantify the uncertainty in publicly available data [6]. The  
 307 reported IC50 values from each dataset were treated as data observations (Equation 10) and the  $\Delta G_{i,target}^{true}$   
 308 was assigned a weak normal prior (Equation 11). The correlation coefficient was calculated for each sample  
 309 according to equation 12. The correlation coefficient  $\rho$  for the CDK2/ERK2 calculations was quantified to  
 310 be  $0.5_{-0.23}^{0.33}$ , indicating that the errors are largely uncorrelated between ERK2 and CDK2 (Figure 5A, right).  
 311 The joint marginal distribution of the error ( $\epsilon$ ) for each target is symmetric, which is expected for cases in  
 312 which  $\rho$  is 0 (Supp. Figure 2). Despite the weak correlation in errors, the high per target accuracy of these  
 313 calculations should have a 2-3x speed up for 1 log unit selectivity optimization, and a 20-30x speed up for  
 314 2 log unit selectivity optimization (Figure 5A, right). The CDK2/CDK9 calculations show strong evidence of  
 315 correlation, with a correlation coefficient of  $0.70_{0.57}^{0.82}$  (Figure 5B, right). The joint marginal distribution of errors  
 316 is strongly diagonal, which is expected based on the value for  $\rho$  (Figure 5B, left). The high correlation in  
 317 errors leads to a speed up of 4-5 for 1 log unit selectivity optimization and 30-40x for 2 log unit selectivity  
 318 optimization (Figure 5B, right), despite the much higher per target errors. Quantifying  $\rho$  for these calculations  
 319 enables estimation of  $\sigma_{selectivity}$ , which is useful for estimating expected error for prospective studies, where  
 320 the experimental values for  $\Delta\Delta G_{selectivity}$  are not yet known. Based on the distribution quantified for  $\rho$ , the  
 321 expected  $\sigma_{selectivity}$  for the CDK2/CDK9 calculations is between 0.76 and 1.16 kcal/mol (Supp. Figure 3), which is  
 322 in good agreement with the bootstrapped RMSE (Figure 4, bottom). For the CDK2/ERK2 calculations,  $\sigma_{selectivity}$   
 323 is expected to fall between 0.82 kcal/mol and 1.10 kcal/mol (Supp. Figure 3), which is also in good agreement  
 324 with the bootstrapped RMSE (Figure 4, top).

325 **Discussion and Conclusions**

326 We have demonstrated, using a simple numerical model, the impact that free energy calculations with even  
 327 weakly correlated errors can have on speeding up the optimization of selectivity in small molecule kinase  
 328 inhibitors. While the expected speed up is dependent on the per target error of the method ( $\sigma_{target}$ ), the  
 329 speedup is also highly dependent on the correlation of errors made for both targets. Unsurprisingly, free  
 330 energy methods have greater impact as the threshold for selectivity optimization goes from 10x to 100x.  
 331 While 100x selectivity optimization is difficult to achieve, the expected benefit from free energy calculations  
 332 is also quite high, with 1 and 2 order of magnitude speedups possible. To quantify the correlation of errors  
 333 in two example systems, we gathered experimental data for two congeneric ligand series with experimental  
 334 data for CDK2 and ERK2, as well as CDK2 and CDK9. These datasets, which had crystal structures for both  
 335 targets with the same ligand co-crystallized, exemplify the difficulty in predicting selectivity. The dynamic  
 336 range of selectivity for both systems is incredibly narrow, with most of the perturbations not having a major  
 337 impact on the overall selectivity achieved. Further, the data was reported with unreliable experimental  
 338 uncertainties, which makes quantifying the errors made by the free energy calculations difficult. This issue is  
 339 common when considering selectivity, as many kinase-oriented high throughput screens are carried out at a  
 340 single concentration and not highly quantitative.

341 discuss quantification of rho (is there a way to know a priori what rho might be?)  
 342 discussion of the expected speedup and sigma based on the quantification of rho  
 343 extensions include: separating statistical error (unless this gets added into the results section)

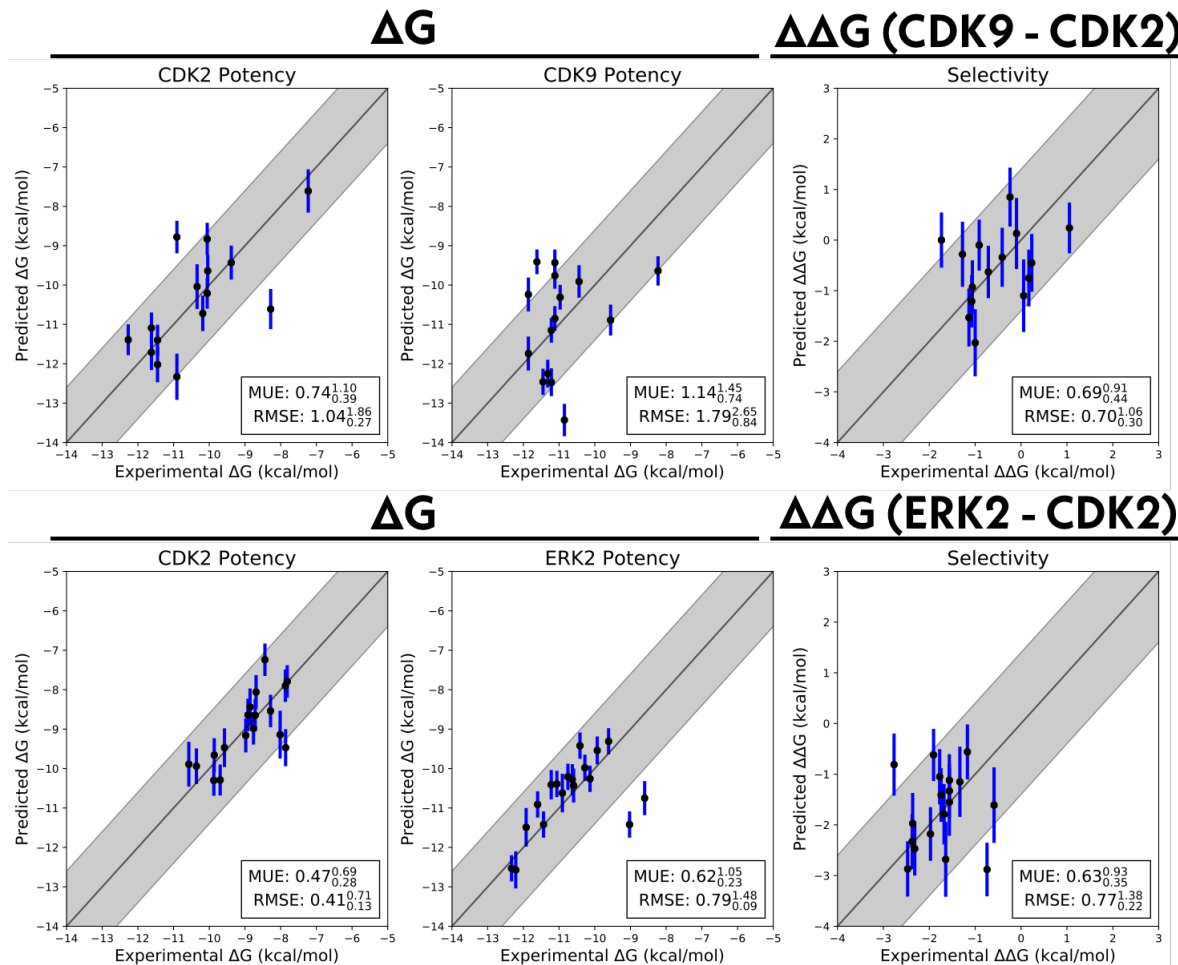


**Figure 4. Relative free energy calculations can accurately predict potency, but show larger errors for selectivity predictions.**

Single target potencies and selectivities for CDK2/ERK2 from the Blake datasets (*top*), and CDK2/CDK9 (*bottom*) from the Shao datasets. The experimental values are shown on the X-axis and calculated values on the Y-axis. Each data point corresponds to a ligand for a given target. All values are shown in units of kcal/mol. The horizontal error bars show the assumed experimental uncertainty of 0.3 kcal/mol[6]. We show the 95% CI based on the estimated statistical ( $\sigma_{stat}$ ) as vertical blue error bars. For selectivity, the errors were propagated under the assumption that they were completely uncorrelated. The black line indicates agreement between calculation and experiment, while the gray shaded region represent 1.36 kcal/mol (or 1 log unit) error. The MUE and RMSE are shown on each plot with bootstrapped 95% confidence intervals.

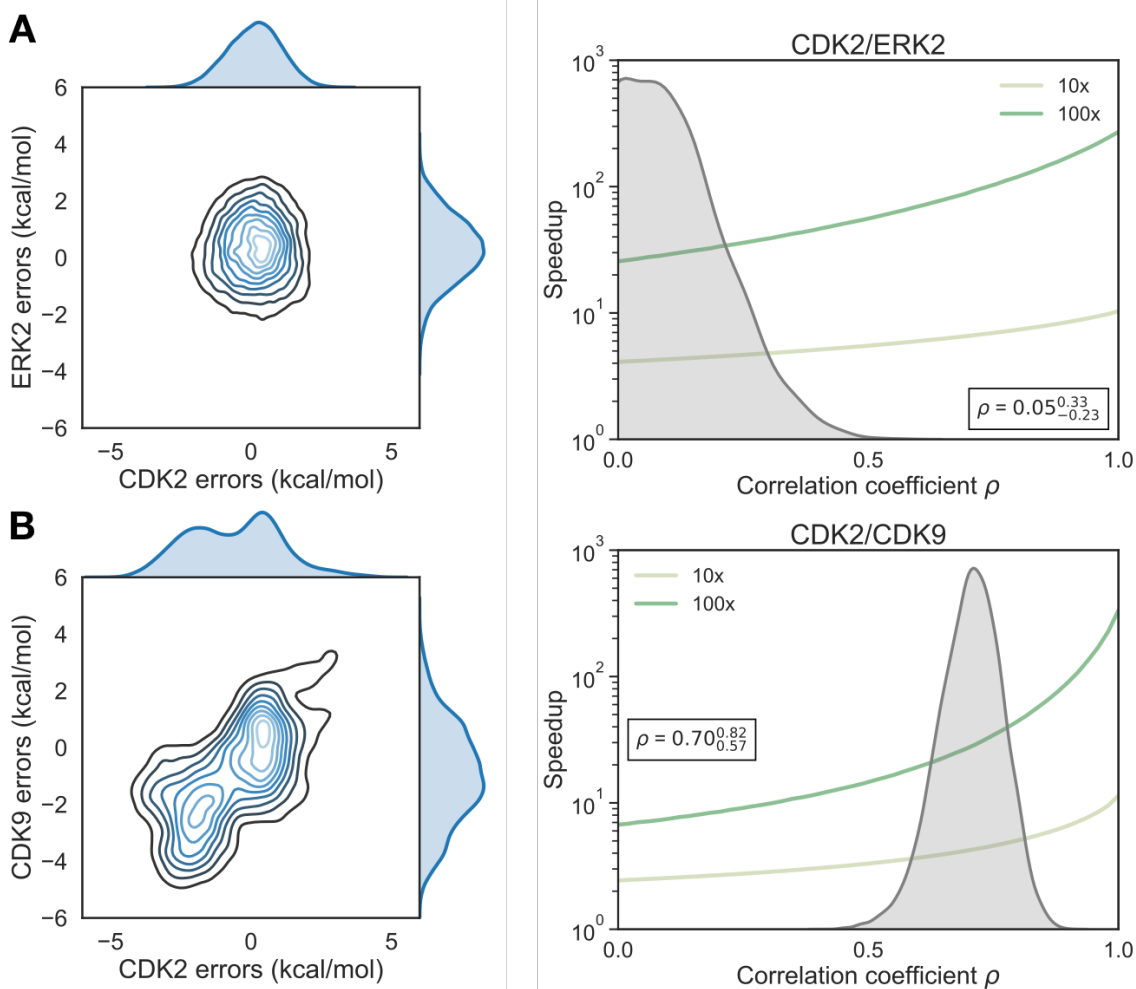


**Figure 5. Correlation in selectivity prediction errors can be used to accelerate selectivity optimization**

(A) (left) The joint posterior distribution of the prediction errors for CDK2 (X-axis) and ERK2 (Y-axis) from the Bayesian graphical model. (right) Speedup in selectivity optimization (Y-axis) as a function of correlation coefficient (X-axis). The posterior marginal distribution of the correlation coefficient ( $\rho$ ) is shown in gray, while the expected speed up is shown for 100x (green curve) and 10x (yellow curve) selectivity optimization. The inserted box shows the mean and 95% confidence interval for the correlation coefficient. (B) (left) The same as above, with CDK2 (X-axis) and CDK9 (Y-axis). (right) As above, for the CDK2/CDK9 calculations.

344 **Acknowledgments**

345 JDC and SKA acknowledge support from NIH grant R01GM121505. JDC acknowledges partial support from  
346 NIH grant P30CA008748.

347 **To be filled out soon**

348 **Disclosures**

349 JDC was a member of the Scientific Advisory Board for Schrödinger, LLC during part of this study. JDC is a  
350 current member of the Scientific Advisory Board of OpenEye Scientific Software. The Chodera laboratory  
351 receives or has received funding from multiple sources, including the National Institutes of Health, the  
352 National Science Foundation, the Parker Institute for Cancer Immunotherapy, Relay Therapeutics, Entasis  
353 Therapeutics, Silicon Therapeutics, EMD Serono (Merck KGaA), AstraZeneca, XtalPi, the Molecular Sciences  
354 Software Institute, the Starr Cancer Consortium, the Open Force Field Consortium, Cycle for Survival, a Louis  
355 V. Gerstner Young Investigator Award, and the Sloan Kettering Institute. A complete funding history for the  
356 Chodera lab can be found at <http://choderlab.org/funding>

357 **Author Contributions**

358 Conceptualization: SKA, LW, RA, JDC  
359 Methodology: SKA, LW, JDC  
360 Investigation: SKA, SP  
361 Writing – Original Draft: SKA  
362 Writing – Review & Editing: SKA, JDC  
363 Funding Acquisition: RA, JDC  
364 Resources: LW, JDC  
365 Supervision: LW, JDC

## 366 References

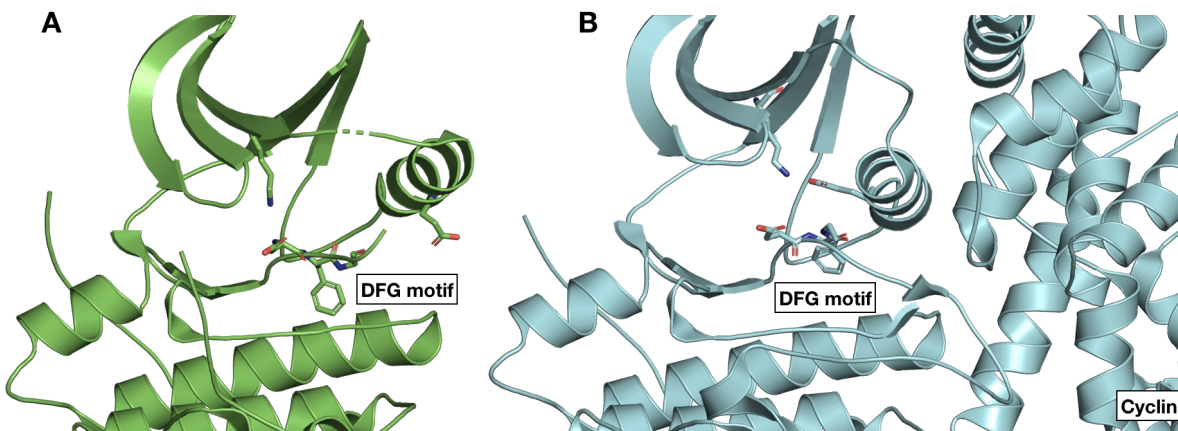
- 367 [1] **Chodera JD**, Mobley DL, Shirts MR, Dixon RW, Branson K, Pande VS. Alchemical free energy methods for drug  
368 discovery: progress and challenges. *Curr Opin Struct Biol.* 2011 Apr; 21(2):150–160.
- 369 [2] **Huang J**, MacKerell AD. CHARMM36 All-Atom Additive Protein Force Field: Validation Based on Comparison to NMR  
370 Data. *J Comput Chem.* 2013 Sep; 34(25):2135–2145. doi: [10.1002/jcc.23354](https://doi.org/10.1002/jcc.23354).
- 371 [3] **Maier JA**, Martinez C, Kasavajhala K, Wickstrom L, Hauser KE, Simmerling C. ff14SB: Improving the Accuracy of  
372 Protein Side Chain and Backbone Parameters from ff99SB. *J Chem Theory Comput.* 2015 Aug; 11(8):3696–3713. doi:  
373 [10.1021/acs.jctc.5b00255](https://doi.org/10.1021/acs.jctc.5b00255).
- 374 [4] **Harder E**, Damm W, Maple J, Wu C, Reboul M, Xiang JY, Wang L, Lupyan D, Dahlgren MK, Knight JL, Kaus JW, Cerutti  
375 DS, Krilov G, Jorgensen WL, Abel R, Friesner RA. OPLS3: A Force Field Providing Broad Coverage of Drug-like Small  
376 Molecules and Proteins. *J Chem Theory Comput.* 2016 Jan; 12(1):281–296. doi: [10.1021/acs.jctc.5b00864](https://doi.org/10.1021/acs.jctc.5b00864).
- 377 [5] **Cournia Z**, Allen B, Sherman W. Relative Binding Free Energy Calculations in Drug Discovery: Recent Advances and  
378 Practical Considerations. *Journal of chemical information and modeling.* 2017 Dec; 57(12):2911–2937.
- 379 [6] **Brown SP**, Muchmore SW, Hajduk PJ. Healthy Skepticism: Assessing Realistic Model Performance. *Drug Discov Today.*  
380 2009; 14(7):420 – 427. doi: <http://dx.doi.org/10.1016/j.drudis.2009.01.012>.
- 381 [7] **Abel R**, Mondal S, Masse C, Greenwood J, Harriman G, Ashwell MA, Bhat S, Wester R, Frye L, Kapeller R, Friesner RA.  
382 Accelerating drug discovery through tight integration of expert molecular design and predictive scoring. *Curr Opin  
383 Struct Biol.* 2017 Apr; 43(Supplement C):38–44.
- 384 [8] **Lovering F**, Aevazeli C, Chang J, Dehnhardt C, Fitz L, Han S, Janz K, Lee J, Kaila N, McDonald J, Moore W, Moretto  
385 A, Papaioannou N, Richard D, Ryan MS, Wan ZK, Thorarensen A. Imidazotriazines: Spleen Tyrosine Kinase (Syk)  
386 Inhibitors Identified by Free-Energy Perturbation (FEP). *ChemMedChem.* 2016 Jan; 11(2):217–233.
- 387 [9] **Ciordia M**, Pérez-Benito L, Delgado F, Trabanco AA, Tresadern G. Application of Free Energy Perturbation for the  
388 Design of BACE1 Inhibitors. *Journal of chemical information and modeling.* 2016 Sep; 56(9):1856–1871.
- 389 [10] **Lenselink EB**, Louvel J, Forti AF, van Veldhoven JPD, de Vries H, Mulder-Krieger T, McRobb FM, Negri A, Goose J, Abel  
390 R, van Vlijmen HWT, Wang L, Harder E, Sherman W, IJzerman AP, Beuming T. Predicting Binding Affinities for GPCR  
391 Ligands Using Free-Energy Perturbation. *ACS omega.* 2016 Aug; 1(2):293–304.
- 392 [11] **Jorgensen WL.** Computer-aided discovery of anti-HIV agents. *Bioorganic & medicinal chemistry.* 2016 Oct;  
393 24(20):4768–4778.
- 394 [12] **Wang L**, Wu Y, Deng Y, Kim B, Pierce L, Krilov G, Lupyan D, Robinson S, Dahlgren MK, Greenwood J, Romero DL, Masse  
395 C, Knight JL, Steinbrecher T, Beuming T, Damm W, Harder E, Sherman W, Brewer M, Wester R, et al. Accurate and  
396 Reliable Prediction of Relative Ligand Binding Potency in Prospective Drug Discovery by Way of a Modern Free-Energy  
397 Calculation Protocol and Force Field. *J Am Chem Soc.* 2015 Feb; 137(7):2695–2703. doi: [10.1021/ja512751q](https://doi.org/10.1021/ja512751q).
- 398 [13] **Abel R**, Wang L, Harder ED, Berne BJ, Friesner RA. Advancing Drug Discovery through Enhanced Free Energy  
399 Calculations. *Accounts of chemical research.* 2017 Jul; 50(7):1625–1632.
- 400 [14] **Zhang J**, Yang PL, Gray NS. Targeting cancer with small molecule kinase inhibitors. *Nat Rev Cancer.* 2009 Jan;  
401 9(1):28–39.
- 402 [15] **Huggins DJ**, Sherman W, Tidor B. Rational approaches to improving selectivity in drug design. *J Med Chem.* 2012 Feb;  
403 55(4):1424–1444.
- 404 [16] **Fan QW**, Cheng CK, Nicolaides TP, Hackett CS, Knight ZA, Shokat KM, Weiss WA. A dual phosphoinositide-3-kinase  
405 alpha/mTOR inhibitor cooperates with blockade of epidermal growth factor receptor in PTEN-mutant glioma. *Cancer  
406 Res.* 2007 Sep; 67(17):7960–7965.
- 407 [17] **Apsel B**, Blair JA, Gonzalez B, Nazif TM, Feldman ME, Aizenstein B, Hoffman R, Williams RL, Shokat KM, Knight ZA.  
408 Targeted polypharmacology: discovery of dual inhibitors of tyrosine and phosphoinositide kinases. *Nat Chem Biol.*  
409 2008 Nov; 4(11):691–699.
- 410 [18] **Knight ZA**, Lin H, Shokat KM. Targeting the Cancer Kinome through Polypharmacology. *Nat Rev Cancer.* 2010;  
411 10(2):130.
- 412 [19] **Hopkins AL**, Mason JS, Overington JP. Can we rationally design promiscuous drugs? *Curr Opin Struct Biol.* 2006 Feb;  
413 16(1):127–136.

- 414 [20] **Hopkins AL.** Network pharmacology: the next paradigm in drug discovery. *Nat Chem Biol.* 2008 Nov; 4(11):682–690.
- 415 [21] **Rudmann DG.** On-target and off-target-based toxicologic effects. *Toxicol Pathol.* 2013 Feb; 41(2):310–314.
- 416 [22] **Kijima T,** Shimizu T, Nonen S, Furukawa M, Otani Y, Minami T, Takahashi R, Hirata H, Nagatomo I, Takeda Y, Kida H, Goya S, Fujio Y, Azuma J, Tachibana I, Kawase I. Safe and successful treatment with erlotinib after gefitinib-induced hepatotoxicity: difference in metabolism as a possible mechanism. *J Clin Oncol.* 2011 Jul; 29(19):e588–90.
- 419 [23] **Liu S,** Kurzrock R. Toxicity of targeted therapy: Implications for response and impact of genetic polymorphisms. *Cancer Treat Rev.* 2014 Aug; 40(7):883–891.
- 420
- 421 [24] **Mendoza MC,** Er EE, Blenis J. The Ras-ERK and PI3K-mTOR pathways: cross-talk and compensation. *Trends Biochem Sci.* 2011 Jun; 36(6):320–328.
- 422
- 423 [25] **Tricker EM,** Xu C, Uddin S, Capelletti M, Ercan D, Ogino A, Pratilas CA, Rosen N, Gray NS, Wong KK, Jänne PA. Combined EGFR/MEK Inhibition Prevents the Emergence of Resistance in EGFR-Mutant Lung Cancer. *Cancer Discov.* 2015 Sep; 5(9):960–971.
- 424
- 425 [26] **Bailey ST,** Zhou B, Damrauer JS, Krishnan B, Wilson HL, Smith AM, Li M, Yeh JJ, Kim WY. mTOR Inhibition Induces Compensatory, Therapeutically Targetable MEK Activation in Renal Cell Carcinoma. *PLoS One.* 2014 Sep; 9(9):e104413.
- 426
- 427 [27] **Chandarlapaty S,** Sawai A, Scaltriti M, Rodrik-Outmezguine V, Grbovic-Huezo O, Serra V, Majumder PK, Baselga J, Rosen N. AKT Inhibition Relieves Feedback Suppression of Receptor Tyrosine Kinase Expression and Activity. *Cancer Cell.* 2011 Jan; 19(1):58–71. doi: 10.1016/j.ccr.2010.10.031.
- 428
- 429
- 430 [28] **Pao W,** Miller V, Zakowski M, Doherty J, Politi K, Sarkaria I, Singh B, Heelan R, Rusch V, Fulton L, Mardis E, Kupfer D, Wilson R, Kris M, Varmus H. EGF receptor gene mutations are common in lung cancers from “never smokers” and are associated with sensitivity of tumors to gefitinib and erlotinib. *Proceedings of the National Academy of Sciences.* 2004 Sep; 101(36):13306–13311.
- 431
- 432
- 433
- 434 [29] **Kim Y,** Li Z, Apetri M, Luo B, Settleman JE, Anderson KS. Temporal resolution of autophosphorylation for normal and oncogenic forms of EGFR and differential effects of gefitinib. *Biochemistry.* 2012 Jun; 51(25):5212–5222.
- 435
- 436
- 437 [30] **Juchum M,** Günther M, Laufer SA. Fighting Cancer Drug Resistance: Opportunities and Challenges for Mutation-Specific EGFR Inhibitors. *Drug Resist Updat.* 2015 May; 20:12–28. doi: 10.1016/j.drup.2015.05.002.
- 438
- 439 [31] **Din OS,** Woll PJ. Treatment of gastrointestinal stromal tumor: focus on imatinib mesylate. *Ther Clin Risk Manag.* 2008 Feb; 4(1):149–162.
- 440
- 441 [32] **Lin YL,** Meng Y, Jiang W, Roux B. Explaining why Gleevec is a specific and potent inhibitor of Abl kinase. *Proc Natl Acad Sci U S A.* 2013 Jan; 110(5):1664–1669.
- 442
- 443 [33] **Lin YL,** Meng Y, Huang L, Roux B. Computational Study of Gleevec and G6G Reveals Molecular Determinants of Kinase Inhibitor Selectivity. *J Am Chem Soc.* 2014 Oct; 136(42):14753–14762.
- 444
- 445 [34] **Lin YL,** Roux B. Computational Analysis of the Binding Specificity of Gleevec to Abl, c-Kit, Lck, and c-Src Tyrosine Kinases. *J Am Chem Soc.* 2013 Oct; 135(39):14741–14753.
- 446
- 447 [35] **Aldeghi M,** Heifetz A, Bodkin MJ, Knapp S, Biggin PC. Predictions of Ligand Selectivity from Absolute Binding Free Energy Calculations. *J Am Chem Soc.* 2017 Jan; 139(2):946–957.
- 448
- 449 [36] **Robert Roskoski Jr.** USFDA Approved Protein Kinase Inhibitors. . 2017; <http://www.brimr.org/PKI/PKIs.htm>, updated 3 May 2017.
- 450
- 451 [37] **Santos R,** Ursu O, Gaulton A, Bento AP, Donadi RS, Bologa CG, Karlsson A, Al-Lazikani B, Hersey A, Oprea TI, Overington JP. A Comprehensive Map of Molecular Drug Targets. *Nat Rev Drug Discov.* 2016 Dec; 16(1):19–34. doi: 10.1038/nrd.2016.230.
- 452
- 453
- 454 [38] **Volkamer A,** Eid S, Turk S, Jaeger S, Rippmann F, Fulle S. Pocketome of human kinases: prioritizing the ATP binding sites of (yet) untapped protein kinases for drug discovery. *J Chem Inf Model.* 2015 Mar; 55(3):538–549.
- 455
- 456 [39] **Manning G,** Whyte DB, Martinez R, Hunter T, Sudarsanam S. The Protein Kinase Complement of the Human Genome. *Science.* 2002 Dec; 298(5600):1912–1934.
- 457
- 458 [40] **Wu P,** Nielsen TE, Clausen MH. FDA-approved small-molecule kinase inhibitors. *Trends Pharmacol Sci.* 2015 Jul; 36(7):422–439.
- 459

- 460 [41] **Cowan-Jacob SW**, Fendrich G, Floersheimer A, Furet P, Liebetanz J, Rummel G, Rheinberger P, Centeleghe M, Fabbro D,  
461 Manley PW, IUCr. Structural biology contributions to the discovery of drugs to treat chronic myelogenous leukaemia.  
462 *Acta Crystallogr D Biol Crystallogr.* 2007 Jan; 63(1):80–93.
- 463 [42] **Seeliger MA**, Nagar B, Frank F, Cao X, Henderson MN, Kuriyan J. c-Src Binds to the Cancer Drug Imatinib with an  
464 Inactive Abl/c-Kit Conformation and a Distributed Thermodynamic Penalty. *Structure.* 2007 Mar; 15(3):299–311.
- 465 [43] **Huse M**, Kuriyan J. The conformational plasticity of protein kinases. *Cell.* 2002 Jan; 109(3):275–282.
- 466 [44] **Harrison SC**. Variation on an Src-like theme. *Cell.* 2003 Mar; 112(6):737–740.
- 467 [45] **Volkamer A**, Eid S, Turk S, Rippmann F, Fulle S. Identification and Visualization of Kinase-Specific Subpockets. *J Chem  
468 Inf Model.* 2016 Feb; 56(2):335–346.
- 469 [46] **Christmann-Franck S**, van Westen GJP, Papadatos G, Beltran Escudie F, Roberts A, Overington JP, Domine D. Un-  
470 precedently Large-Scale Kinase Inhibitor Set Enabling the Accurate Prediction of Compound-Kinase Activities: A Way  
471 toward Selective Promiscuity by Design? *Journal of chemical information and modeling.* 2016 Sep; 56(9):1654–1675.
- 472 [47] **Anastassiadis T**, Deacon SW, Devarajan K, Ma H, Peterson JR. Comprehensive assay of kinase catalytic activity  
473 reveals features of kinase inhibitor selectivity. *Nat Biotechnol.* 2011 Nov; 29(11):1039–1045.
- 474 [48] **Davis MI**, Hunt JP, Herrgard S, Ciceri P, Wodicka LM, Pallares G, Hocker M, Treiber DK, Zarrinkar PP. Comprehensive  
475 Analysis of Kinase Inhibitor Selectivity. *Nat Biotechnol.* 2011 Oct; 29(11):1046–1051. doi: [10.1038/nbt.1990](https://doi.org/10.1038/nbt.1990).
- 476 [49] **Klaeger S**, Heinzlmeir S, Wilhelm M, Polzer H, Vick B, Koenig PA, Reinecke M, Ruprecht B, Petzoldt S, Meng C, Zecha  
477 J, Reiter K, Qiao H, Helm D, Koch H, Schoof M, Canevari G, Casale E, Depaolini SR, Feuchtinger A, et al. The target  
478 landscape of clinical kinase drugs. *Science.* 2017 Dec; 358(6367).
- 479 [50] **Sun C**, Hobor S, Bertotti A, Zecchin D, Huang S, Galimi F, Cottino F, Prahallas A, Grernrum W, Tzani A, Schlicker A,  
480 Wessels LFA, Smit EF, Thunnissen E, Halonen P, Lieftink C, Beijersbergen RL, Di Nicolantonio F, Bardelli A, Trusolino L,  
481 et al. Intrinsic resistance to MEK inhibition in KRAS mutant lung and colon cancer through transcriptional induction  
482 of ERBB3. *Cell Reports.* 2014 Apr; 7(1):86–93.
- 483 [51] **Manchado E**, Weissmueller S, Morris JP, Chen CC, Wullenkord R, Lujambio A, de Stanchina E, Poirier JT, Gainor JF,  
484 Corcoran RB, Engelman JA, Rudin CM, Rosen N, Lowe SW. A combinatorial strategy for treating KRAS-mutant lung  
485 cancer. *Nature.* 2016 Jun; 534(7609):647–651.
- 486 [52] **Shao H**, Shi S, Huang S, Hole AJ, Abbas AY, Baumli S, Liu X, Lam F, Foley DW, Fischer PM, Noble M, Endicott JA, Pepper  
487 C, Wang S. Substituted 4-(Thiazol-5-yl)-2-(phenylamino)pyrimidines Are Highly Active CDK9 Inhibitors: Synthesis, X-ray  
488 Crystal Structures, Structure–Activity Relationship, and Anticancer Activities. *J Med Chem.* 2013 Feb; 56(3):640–659.
- 489 [53] **Blake JF**, Burkard M, Chan J, Chen H, Chou KJ, Diaz D, Dudley DA, Gaudino JJ, Gould SE, Grina J, Hunsaker T, Liu L,  
490 Martinson M, Moreno D, Mueller L, Orr C, Pacheco P, Qin A, Rasor K, Ren L, et al. Discovery of (S)-1-(1-(4-Chloro-3-  
491 fluorophenyl)-2-hydroxyethyl)-4-(2-((1-methyl-1H-pyrazol-5-yl)amino)pyrimidin-4-yl)pyridin-2(1H)-one (GDC-0994),  
492 an Extracellular Signal-Regulated Kinase 1/2 (ERK1/2) Inhibitor in Early Clinical Development. *J Med Chem.* 2016 Jun;  
493 59(12):5650–5660.
- 494 [54] **Hole AJ**, Baumli S, Shao H, Shi S, Huang S, Pepper C, Fischer PM, Wang S, Endicott JA, Noble ME. Comparative Structural  
495 and Functional Studies of 4-(Thiazol-5-yl)-2-(phenylamino)pyrimidine-5-carbonitrile CDK9 Inhibitors Suggest the Basis  
496 for Isootype Selectivity. *J Med Chem.* 2013 Feb; 56(3):660–670.
- 497 [55] **Berman HM**, Battistuz T, Bhat TN, Bluhm WF, Bourne PE, Burkhardt K, Feng Z, Gilliland GL, Iype L, Jain S, Fagan P,  
498 Marvin J, Padilla D, Ravichandran V, Schneider B, Thanki N, Weissig H, Westbrook JD, Zardecki C. The Protein Data  
499 Bank. *Acta Crystallogr D Biol Crystallogr.* 2002 Jun; 58(Pt 61):899–907.
- 500 [56] **Sastry GM**, Adzhigirey M, Day T, Annabhimoju R, Sherman W. Protein and ligand preparation: parameters, protocols,  
501 and influence on virtual screening enrichments. *J Comput Aided Mol Des.* 2013 Mar; 27(3):221–234.
- 502 [57] **Harder E**, Damm W, Maple J, Wu C, Reboul M, Xiang JY, Wang L, Lupyan D, Dahlgren MK, Knight JL, Kaus JW, Cerutti  
503 DS, Krilov G, Jorgensen WL, Abel R, Friesner RA. OPLS3: A Force Field Providing Broad Coverage of Drug-like Small  
504 Molecules and Proteins. *J Chem Theory Comput.* 2016 Jan; 12(1):281–296.
- 505 [58] **Abel R**, Wang L, Harder ED, Berne BJ, Friesner RA. Advancing Drug Discovery through Enhanced Free Energy  
506 Calculations. *Acc Chem Res.* 2017 Jul; 50(7):1625–1632. doi: [10.1021/acs.accounts.7b00083](https://doi.org/10.1021/acs.accounts.7b00083).

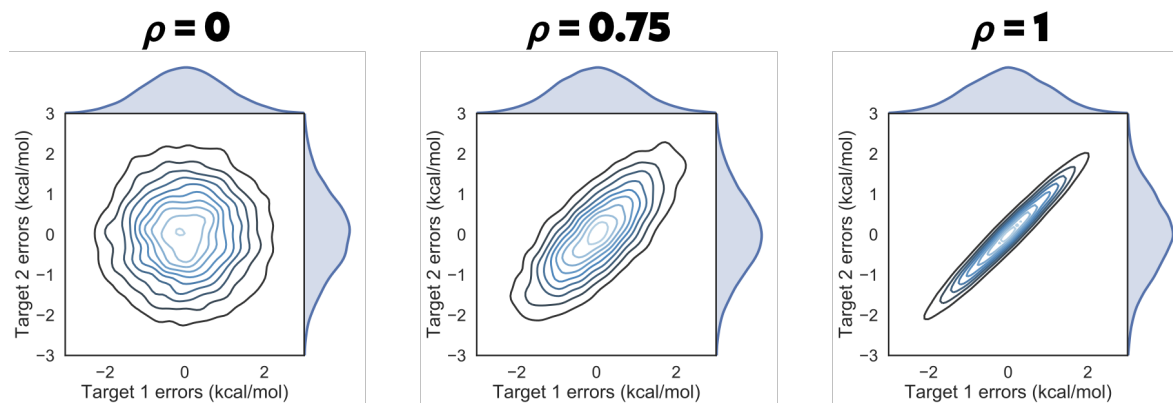
- 507 [59] **Bochevarov AD**, Harder E, Hughes TF, Greenwood JR, Braden DA, Philipp DM, Rinaldo D, Halls MD, Zhang J, Friesner  
508 RA. Jaguar: a high-performance quantum chemistry software program with strengths in life and materials sciences.  
509 Int J Quantum Chem. 2013; 113(18):2110–2142.
- 510 [60] **Salvatier J**, Wiecki TV, Fonnesbeck C. Probabilistic programming in Python using PyMC3. PeerJ Computer Science.  
511 2016; 2:e55.
- 512 [61] **Al-Rfou R**, Alain G, Almahairi A, Angermueller C, Bahdanau D, Ballas N, Bastien F, Bayer J, Belikov A, Belopolsky A,  
513 Bengio Y, Bergeron A, Bergstra J, Bisson V, Bleecher Snyder J, Bouchard N, Boulanger-Lewandowski N, Bouthillier X,  
514 de Brébisson A, Breuleux O, et al. Theano: A Python framework for fast computation of mathematical expressions.  
515 arXiv e-prints. 2016 May; abs/1605.02688. <http://arxiv.org/abs/1605.02688>.
- 516 [62] **Bosc N**, Meyer C, Bonnet P. The use of novel selectivity metrics in kinase research. BMC bioinformatics. 2017 Jan;  
517 18(1):17.
- 518 [63] **Cheng AC**, Eksterowicz J, Geuns-Meyer S, Sun Y. Analysis of kinase inhibitor selectivity using a thermodynamics-based  
519 partition index. J Med Chem. 2010 Jun; 53(11):4502–4510.
- 520 [64] **Hauser K**, Negron C, Albanese SK, Ray S, Steinbrecher T, Abel R, Chodera JD, Wang L. Predicting resistance of clinical  
521 Abl mutations to targeted kinase inhibitors using alchemical free-energy calculations. Communications Biology. 2018  
522 Jun; 1(1):70.
- 523 [65] **Hari SB**, Merritt EA, Maly DJ. Sequence determinants of a specific inactive protein kinase conformation. Chemistry &  
524 biology. 2013 Jun; 20(6):806–815.
- 525 [66] **Hu J**, Ahuja LG, Meharena HS, Kannan N, Kornev AP, Taylor SS, Shaw AS. Kinase regulation by hydrophobic spine  
526 assembly in cancer. Molecular and cellular biology. 2015 Jan; 35(1):264–276.

527 **Supplemental Information**

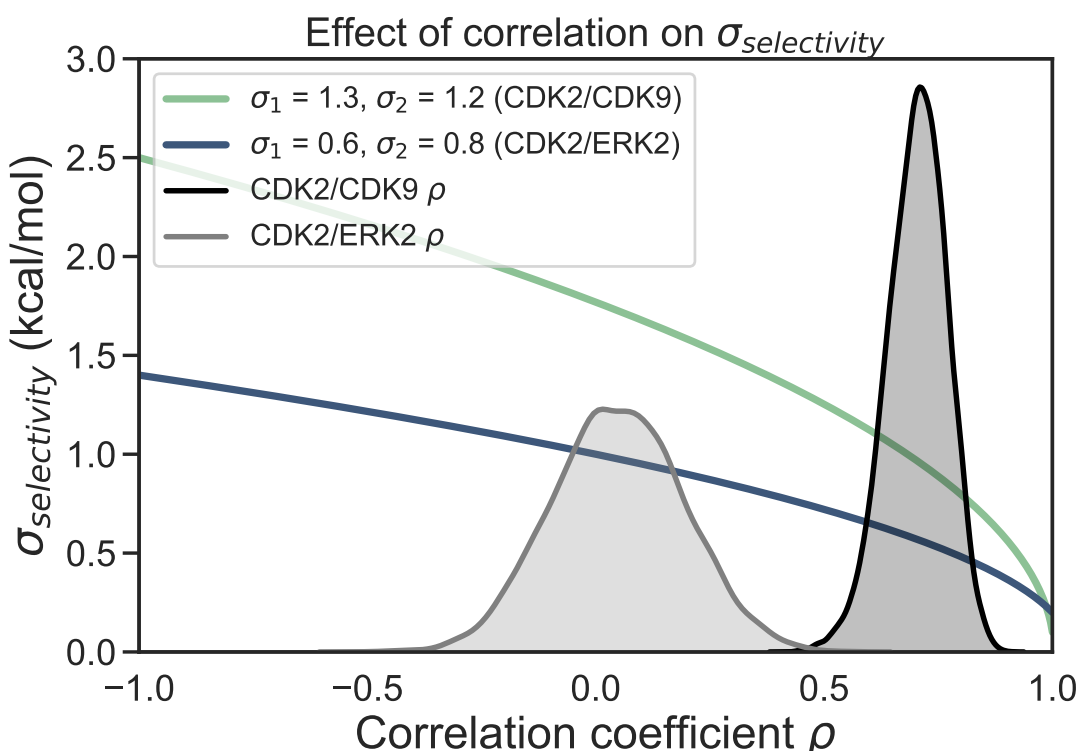


**Supplemental Figure 1.** CDK2 adopts an inactive conformation in the crystal structure used for the CDK2/ERK2 calculations

(A) CDK2 (5K4J) adopts an inactive conformation in the absence of its cyclin. The DFG motif is in a DFG-out conformation, with the  $\alpha$ C helix rotated outwards, breaking the salt bridge between K33 and E51 (Uniprot numbering) that is typically a marker of an active conformation. Notably, the Phe in the DFG motif does not completely form the hydrophobic spine due to the rotation of the  $\alpha$ C helix [66] (B) The CDK2 structure used for the CDK2/CDK9 calculations (4BCK) contains cyclin A and adopts a DFG-in/ $\alpha$ C helix-in conformation that forms the salt bridge between K33 and E51. This is typically indicative of a fully active kinase [43, 65].

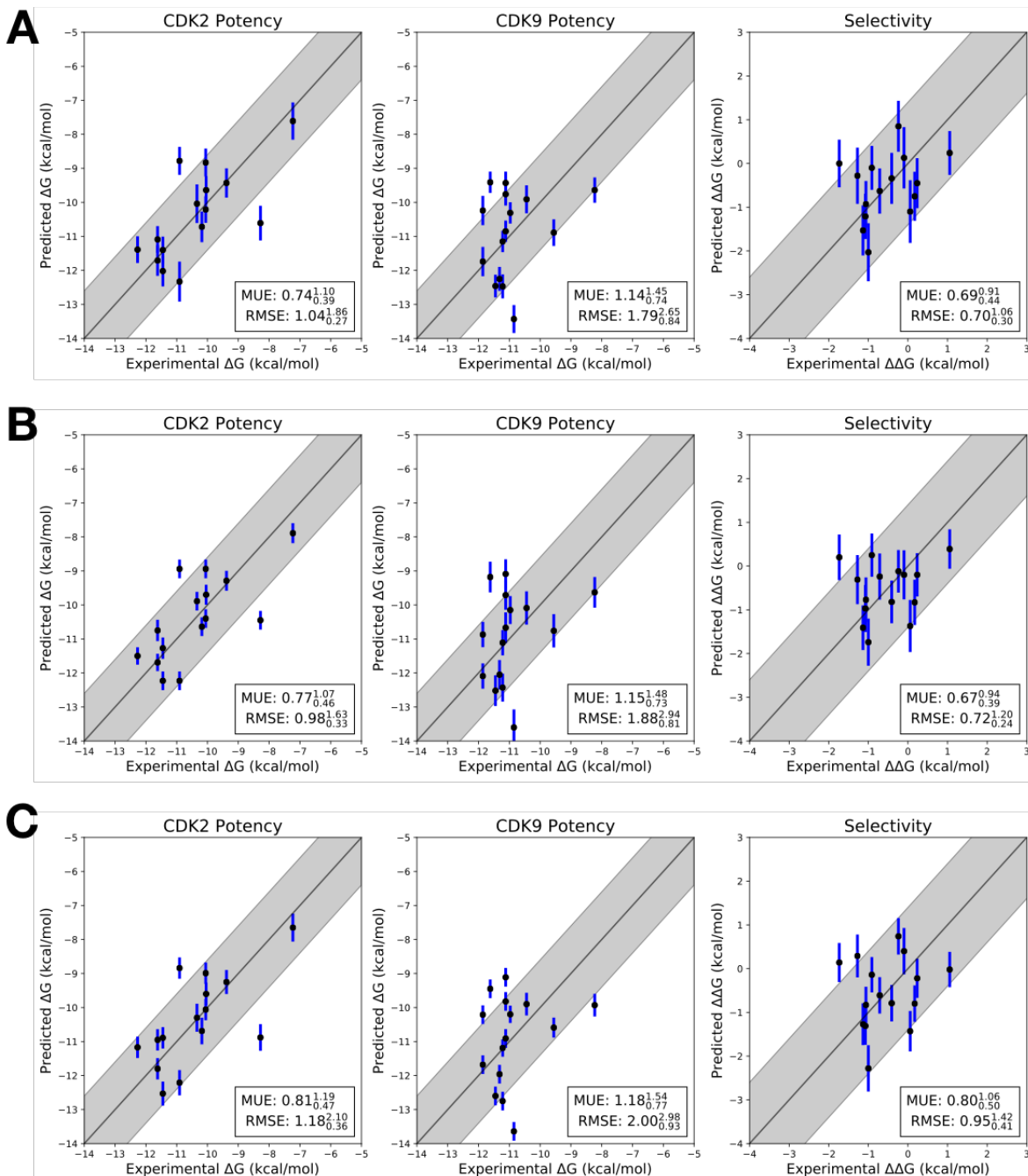


**Supplemental Figure 2. Correlation coefficient  $\rho$  controls the shape of the joint marginal distribution of errors**  
As  $\rho$  increases, the joint marginal distribution of errors become more diagonal. Each panel shows 10000 samples drawn from a multivariate normal distribution centered around 0 kcal/mol, where the per target error was set to 1 kcal/mol and  $\rho$  to the value indicated in bold over the plot.

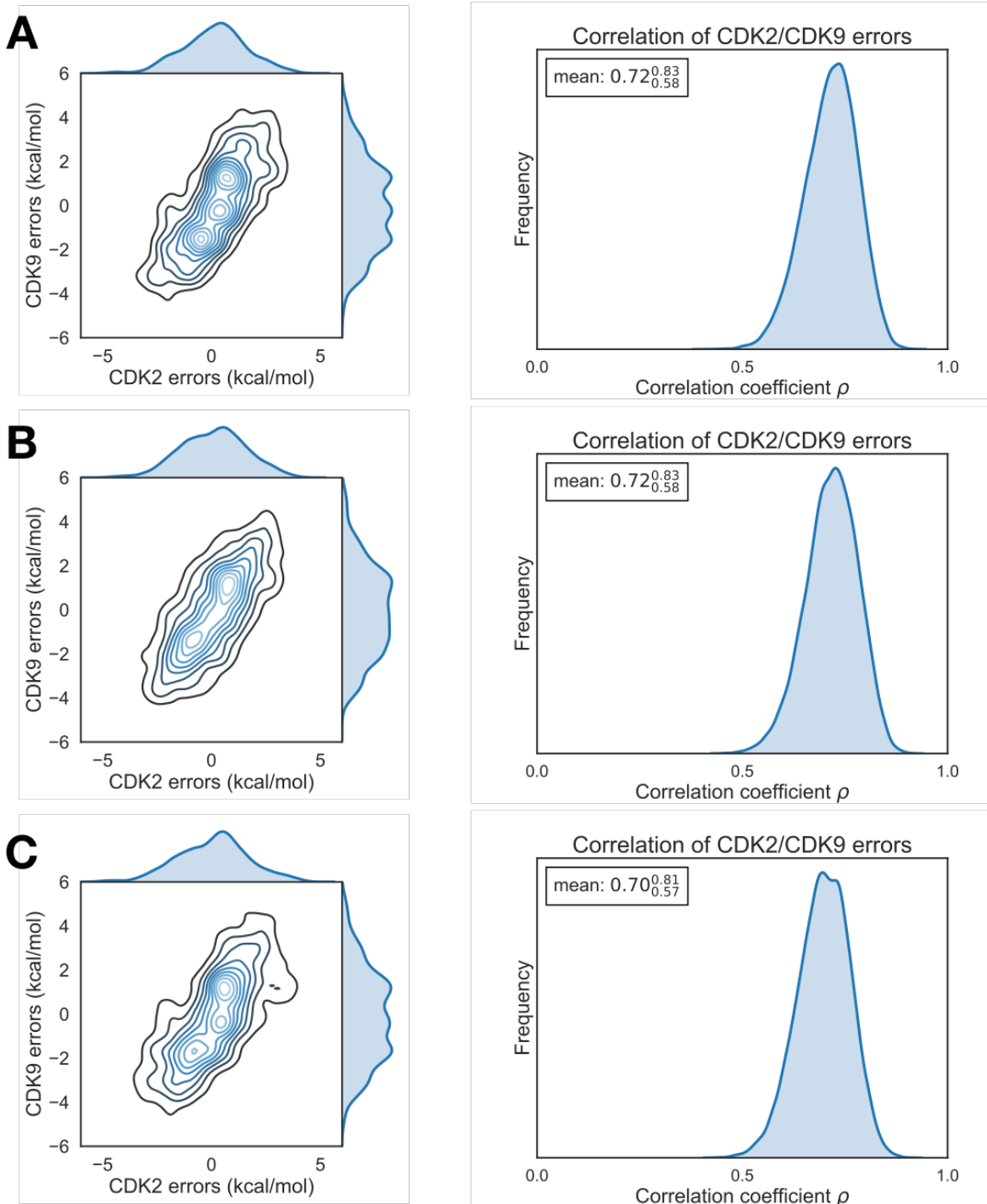


**Supplemental Figure. 3. Correlation reduces the expected error for selectivity predictions**

As corelation coefficient  $\rho$  increases,  $\sigma_{selectivity}$  decreases. The intersection between CDK2/CDK9  $\sigma_{selectivity}$  (green curve) and  $\rho$  (black distribution) indicates the range of expected  $\sigma_{selectivity}$  values. The intersection for CDK2/ERK  $\sigma_{selectivity}$  (blue curve) and  $\rho$  (gray distribution) suggests the expected  $\sigma_{selectivity}$  range for that set of calculations.

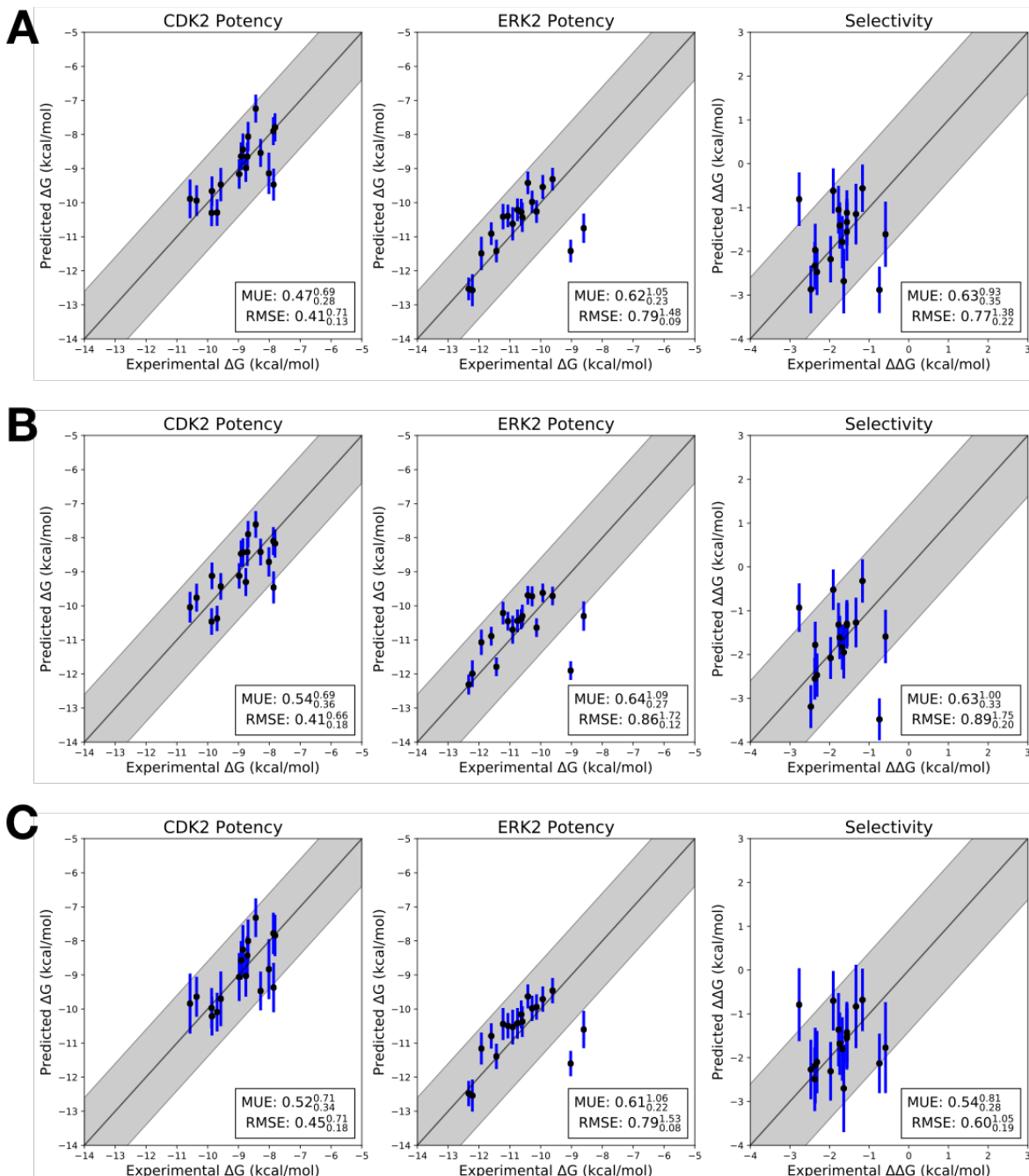
**Supplemental Figure. 4. Each replicate of the CDK2/CDK9 calculations yields a consistent RMSE and MUE**

Three replicates of the CDK2/CDK9 calculations with different random seeds, but otherwise the same input structures, files, and parameters. The experimental values are shown on the X-axis and calculated values on the Y-axis. Each data point corresponds to a ligand for a given target. All values are shown in units of kcal/mol. The horizontal error bars show the assumed experimental uncertainty of 0.3 kcal/mol[6]. We show the 95% CI based on the estimated statistical as vertical blue error bars. For selectivity, the errors were propagated under the assumption that they were completely uncorrelated. The black line indicates agreement between calculation and experiment, while the gray shaded region represent 1.36 kcal/mol (or 1 log unit) error. The MUE and RMSE are shown on each plot with bootstrapped 95% confidence intervals. (**A**) Replicate 1 (**B**) Replicate 2 (**C**) Replicate 3



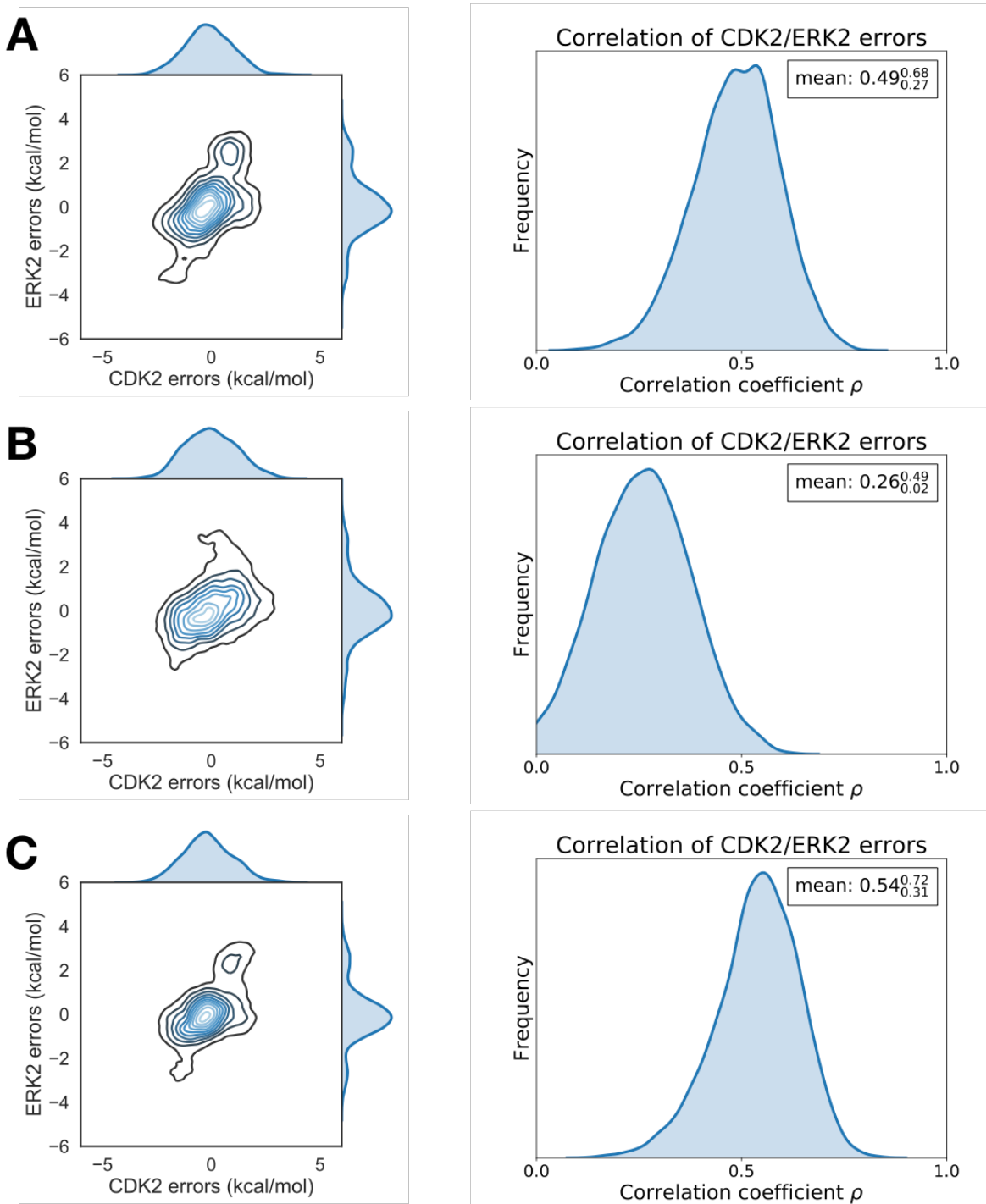
**Supplemental Figure 5. Each replicate of the CDK2/CDK9 calculations yields consistent errors and correlation coefficient**

(A) (left) The joint posterior distribution of the prediction errors for CDK2 (X-axis) and CDK9 (Y-axis) from the Bayesian graphical model for replicate 1. (right) The posterior marginal distribution of the correlation coefficient ( $\rho$ ) is shown in gray for replicate 1. The inserted box shows the mean and 95% confidence interval for the correlation coefficient. (B) and (C) The same as above, but for replicates 2 and 3, respectively



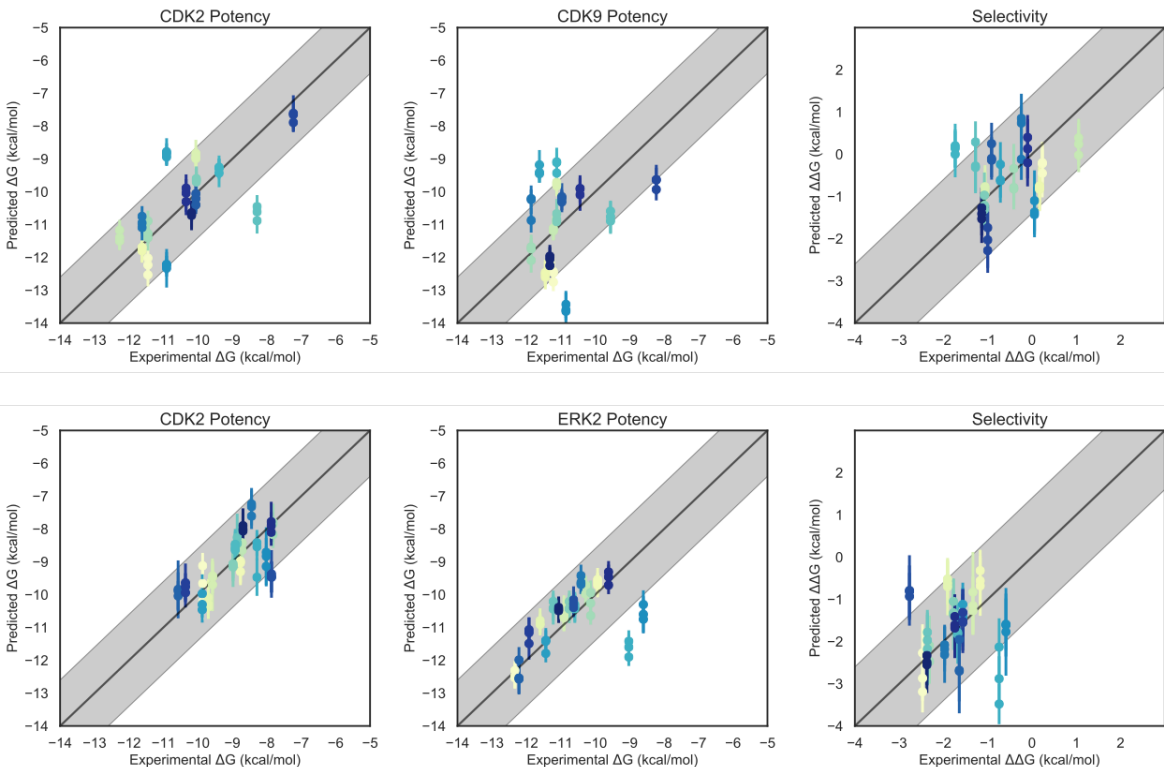
**Supplemental Figure. 6. Each replicate of the CDK2/ERK2 calculations yields a consistent RMSE and MUE**

Three replicates of the CDK2/ERK2 calculations with different random seeds, but otherwise the same input structures, files, and parameters. The experimental values are shown on the X-axis and calculated values on the Y-axis. Each data point corresponds to a ligand for a given target. All values are shown in units of kcal/mol. The horizontal error bars show the assumed experimental uncertainty of 0.3 kcal/mol [6]. We show the 95% CI based on the estimated statistical as vertical blue error bars. For selectivity, the errors were propagated under the assumption that they were completely uncorrelated. The black line indicates agreement between calculation and experiment, while the gray shaded region represent 1.36 kcal/mol (or 1 log unit) error. The MUE and RMSE are shown on each plot with bootstrapped 95% confidence intervals. (**A**) Replicate 1 (**B**) Replicate 2 (**C**) Replicate 3



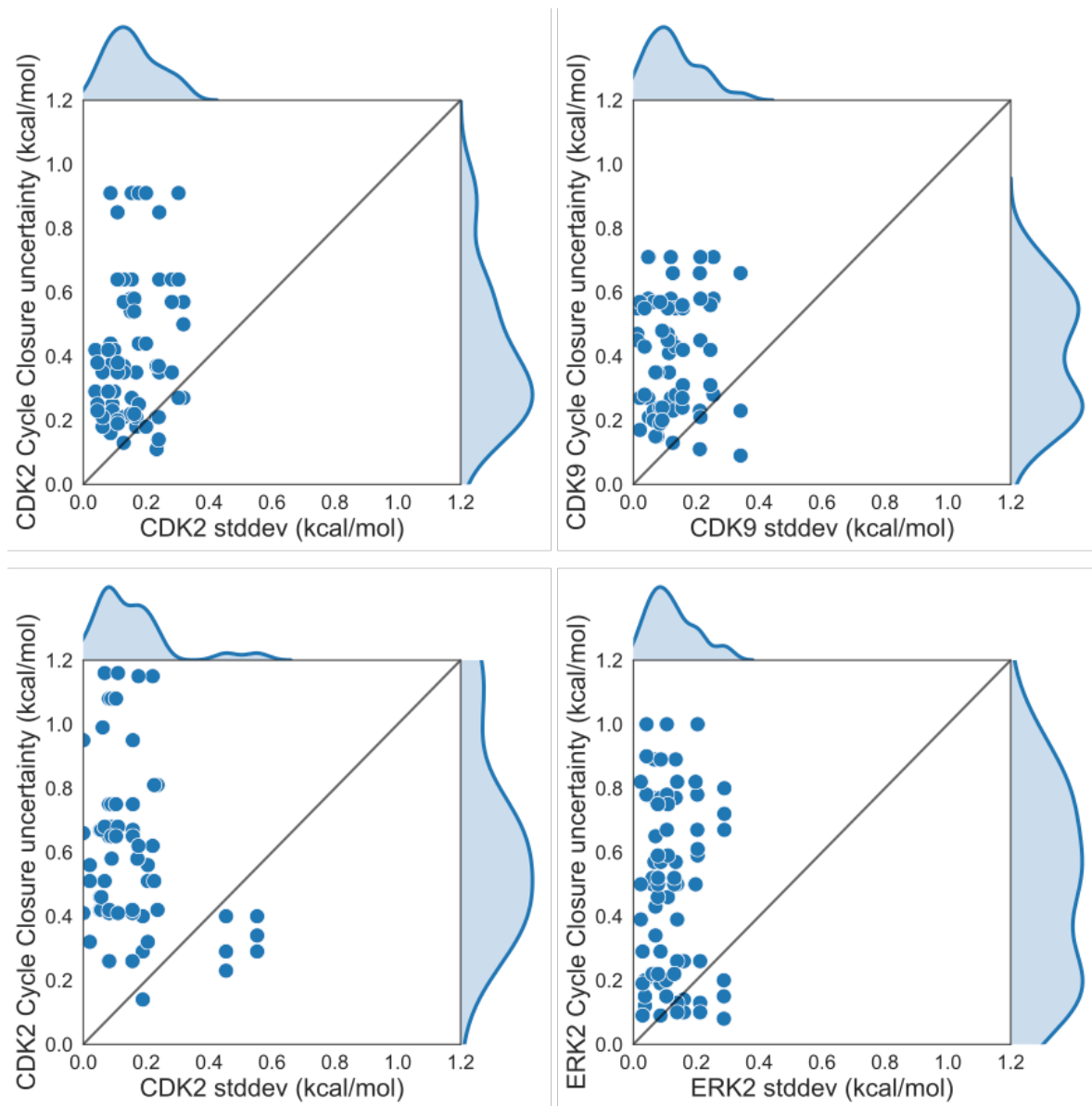
**Supplemental Figure 7. Each replicate of the CDK2/ERK2 calculations yields consistent errors and correlation coefficient**

(A) (left) The joint posterior distribution of the prediction errors for CDK2 (X-axis) and ERK2 (Y-axis) from the Bayesian graphical model for replicate 1. (right) The posterior marginal distribution of the correlation coefficient ( $\rho$ ) is shown in gray for replicate 1. The inserted box shows the mean and 95% confidence interval for the correlation coefficient. (B) and (C) The same as above, but for replicates 2 and 3, respectively



**Supplemental Figure. 8. The pooled replicates show good agreement in predictions for individual ligands**

The experimental values are shown on the X-axis and calculated values on the Y-axis. Each data point corresponds to a ligand for a given target. All values are shown in units of kcal/mol. The horizontal error bars show the assumed experimental uncertainty of 0.3 kcal/mol[6]. We show the 95% CI based on the estimated statistical as vertical blue error bars. For selectivity, the errors were propagated under the assumption that they were completely uncorrelated. The black line indicates agreement between calculation and experiment, while the gray shaded region represent 1.36 kcal/mol (or 1 log unit) error. The MUE and RMSE are shown on each plot with bootstrapped 95% confidence intervals. (**Top**) CDK2/CDK9 replicates (**Bottom**) CDK2/ERK2 replicates



**Supplemental Figure. 9. The standard deviation for each edge is smaller than the estimated cycle closure uncertainties**

The cycle closure uncertainty for each edge of the map is shown on the Y-axis and the standard deviation for that edge in all three replicate calculations is shown on the X-axis, in kcal/mol. Each point corresponds to an edge of the FEP map. The edges for all three replicates are pooled and shown together. (**Top**) CDK2/CDK9 calculations (**Bottom**) CDK2/ERK2 calculations.